N86-11095

FINAL REPORT

TITLE: Theoretical Analysis of Wolter/LSM X-Ray Telescope Systems

AUTHORS: D. L. Shealy, S. Chao

PURCHASE ORDER NO: H-78183B

PERIOD: October 1, 1984 - May 26, 1985

DATE OF PUBLICATION: October 1, 1985

PRINCIPAL INVESTIGATOR: David L. Shealy, Ph.D.
Physics Department
Physical Sciences Bldg., Room 227
University of Alabama at Birmingham
205-934-4736

PREPARED FOR: George C. Marshall Space Flight Center
Marshall Space Flight Center, Alabama 35812

DISTRIBUTION (19 copies + repro)
0/AP29-H (Letter of Transmittal)
5/AS24D
1/AT01
1/CC01/Wofford
10 + repro/EM13A-19
1/ES 52 (Attn: R.B. Hoover)
NASA Scientific and Technical Information
Facility (1 copy + repro)

ABSTRACT

A ray tracing analysis has been performed for the spectral slicing zoom x-ray telescope for configurations in which a convex layered synthetic microstructure (LSM) optic is placed in front of the prime focus or a concave LSM optic is placed behind the prime focus. The analysis has considered the geometrical shape of the LSM optic to be either a hyperboloid, sphere, ellipsoid or constant optical path aspheric element for two configurations of the glancing incidence x-ray telescope: the ATM Experimental S-056 Wolter I system and the Stanford/MSFC Wolter-Schwarzchild nested system. For the different systems the RMS blur circle radii, the point spread function (PSF), the full width half maximum (FWHM) of the PSF have been evaluated as a function of field angle and magnification of the secondary to determine resolution of the system. The effects of decentration and tilt of the selected LSM element on the performance of the system have been studied to determine mounting and alignment tolerances. It has been shown that the spherical LSM optic should yeild sub arc second performance over the entire field of view (16 arc minutes). Critical mirror parameters required for fabrication have been determined.

TABLE OF CONTENTS

INTRODUCTION*

Over the past two decades, numerous glancing incidence x-ray telescopes have been fabricated and flown on sounding rockets and satellites to produce high-resolution images of the Sun and cosmic x-ray sources. The optics for these telescopes usually involve conic surfaces of revolution, which were first described by H. Wolter[1] in 1952 as systems for aplanatic x-ray microscopes. Subsequently, Wolter[2] modified the Schwarzschild[3] general equations for two-element reflecting telescopes. These Wolter-Schwarzschild systems generally yield slightly improved performance at the larger field angles, but the mirrors are more complex and difficult to fabricate. Wolter Type I optics (Figure 1), where internally reflecting paraboloid is followed by an internally reflecting hyperboloid, has been the most extensively used imaging system for x-ray telescopes designed to operate in the 3 - 100 Å region. (See Hoover, Thomas, and Underwood[4] for a general review of the principles of glancing incidence x-ray optics.) Nested Wolter I mirrors were utilized on the Einstein Observatory[5] (which revolutionized cosmic x-ray astronomy) and are being planned for the Advanced X-Ray Astrophysics Facility (AXAF).[6]

Our knowledge of solar x-ray phenomena was dramatically increased in 1973 by Wolter I telescopes carried aboard the Apollo Telescope Mount (ATM) on the Skylab mission. During this mission, ATM experiments S-056 (MSFC) and S-054 (American Science & Engineering) produced over 70,000 high-resolution x-ray images that provided a wealth of information

*The results of this study were presented to the SPIE Symposium on the Applications of Thin-Film Multilayered Structures to Figures X-Ray Optics on August 20-22, 1985 and were published in Ref. 16. A reprint of this paper is enclosed in Appendix A.

regarding solar flares, coronal holes, and x-ray bright points. Both of these telescopes employed photographic emulsions as x-ray detectors, and the film magazines were removed by the astronauts and returned to Earth for processing and analysis. While photographic emulsions afford higher spatial resolution than can be presently obtained with solid state detectors such as CCD's, film has a much lower sensitivity. Film also has the disadvantage that it must be retrieved and developed before analysis. This makes film an unsuitable detector for us on many unmanned satellites and observatories.

It is now well established that glancing incidence Wolter I x-ray telescopes have a sharply peaked point response function and that the spatial resolution realized with these systems is in general limited by the detector. For example, solar x-ray images recorded by ATM Experiment S-056 with a 1.9 m focal length (plate scale 9 m/arc second) exhibited a resolution limit of 2.2 arc seconds on SO-212 film (uncoated Panatomic-X) and 1.8 arc seconds on SO-242 film. However, in laboratory tests using Kodak High-Resolution Photographic Plates, spatial resolution of 0.75-0.8 arc seconds was achieved with these flight optics.[7] Hence, limitations of the spatial resolution imposed even by high-resolution detectors such as film may degrade the performance of state-of-the-art x-ray telescopes. Far more severe degradations would be experienced with solid state detectors, which afford much higher sensitivity over broader spectral ranges but currently have lower spatial resolution than can be achieved with photographic film. Technological limitations presently make it impossible to fabricate solid state detectors with pixel sizes much smaller than 10 m. Better resolution with these devices can be realized with telescopes of longer focal length and therefore increased plate scale. However, these instruments are of necessity heavier and more costly, and may exceed the

envelopes allowed by some sounding rockets and satellites.

For these reasons, various techniques for using auziliary optics to increase the plate scale without significantly increasing the telescope physical length have been studied. Chase et al.[8] investigated Grazing Incidence Relay Optics (GIRO) as a means of coupling x-ray mirror systems to detectors. In the MSFC Extended Range X-Ray Telescope (ERXRT) program, several glancing incidence hyperboloid/ellipsoid x-ray microscope optics of different magnifications and focal lengths were designed and anlyzed.[9,10] The studies optimized an x-ray microscope optic (8x) for use in coupling the ATM Experiment S-056 x-ray optics to a CCD of 30 μm pixel size. The ERXRT with a 4-meter telescope possesses a plate scale that would normally require an instrument 16 meters long. Ray trace results indicate that sub arc second performance should be achievable over the entire 4 arc minute field-of-view afforded by the 320x512 x-ray sensitive area of the RCA CCD. Since the microscope optics can be configured to operate at glancing angles similar to the primary, it is possible to reflect x-rays over the entire spectral range covered by the Wolter x-ray optics. Although x-ray microscope optics are expensive and difficult to fabricate and the image quality and throughput degrades fairly rapidly with field angle, these optics should be of great value for high-resolution imaging of selected features over braod spectral ranges and for use in conjunction with high-resolution x-ray spectrometers.

An alternative system for realizing the high inherent resolution capability of the Wolter optics without significantly increasing the telescope physical length should be achieved by the use of Layered Synthetic Microstructure (LSM) optics.[11-14] As determined by the optical properties and thickness of the multilayers, the LSMs can be tailored to reflect only specific narrow spectral slices of the incident

x-ray beam. By the use of normal incidence LSM optics on properly contoured sybstrates, spectral slicing x-ray telescope systems with variable magnifications may be realized (Figure 2). Variable magnification would allow the instrument to shift from moderate resolution x-ray images of the entire solar disk to very high-resolution images of selected active regions, loops, bright points, or other features of interest. The narrow bandpasses afforded by properly designed LSM optics should permit far superior plasma diagnostics to be performed than was possible from the crude filtergrams obtained during the Skylab mission. Since it is unnecessary to increase the physical length of the instrument, these systems should be ideal for sounding rockets and many satellites that have limitations with regard to the size of payload that can be accommodated.

Presented in this study (see Appendix B for Work Statement) are the results of our theoretical investigations of spectral slicing x-ray telescope systems in which the ATM Experiment S-056 Wolter I optics and the nested Wolter-Schwarzschild mirrors from the Stanford/MSFC Rocket Experiment are considered as the primary optics. The basic optical parameters for these mirrors are presented in Table 1. The performance of these systems was evaluated for LSM optics of hyperboloidal, spherical, ellipsoidal, and constant optical path aspheric configurations. We have calculated the RMS blur circle radii, the point response functions, and the full width half maxima of the line spread functions to establish the resolution theoretically attainable. The percent energy loss as a function of field angle was also established by ray trace procedures.

MATHEMATICAL ANALYSIS OF THE SPECTRAL SLICING X-RAY TELESCOPE

The Spectral Slicing X-Ray Telescope is based upon the concept of using normal incidence contoured LSM optics to reflect and magnify a narrow spectral slice of the x-ray image produced by the primary mirrors. As is seen in Fig. 3, this can be accomplished by means of either convex LSM mirrors placed in front of the prime focus or concave LSM optics behind the focus. The x-rays are reflected by the LSM optics to form a magnified image on the detector located at Z_I on the Z-axis. The design condition requires that an on-axis incident ray that strikes the intersection (R_2,Z_2) of the primary Wolter optics be reflected by the LSM optics to form an image at the detector. The geometry of the Spectral Slicing X-Ray Telescope is shown in Fig. 4. The surface parameters of the LSM optics are determined by the design condition and the LSM surface equation. The results are expressed in terms of the magnification of the LSM mirror. (See Appendix A for equations required to calculate the LSM mirror parameters).

Numerical values for spherical LSM radius and vertex location, R_3 and Z_{03}, for the configuration of the S-056 primary with a convex LSM spherical optics are as follows.

M	R (cm)	Z (cm)
2	269.94	257.88
6	69.37	219.37
8	51.38	212.95

The Wolter-Schwarzschild/convex spherical LSM values are:

M	R (cm)	Z (cm)
2	204.89	51.22
6	52.88	22.03
8	39.71	17.37

Numerical values for the concave ellipsoidal LSM-S056 mirror parameters are given below:

M	A (cm)	B (cm)	C (cm)
2	303.38	286.02	101.12
6	141.57	99.08	101.12
8	130.01	81.72	101.12

Numerical values for the convex hyperboloidal LSM-S056 mirror parameters are are follows:

M	A (cm)	B (cm)	C (cm)
2	33.70	95.34	101.12
6	72.23	70.77	101.12
8	78.65	63.56	101.12

For a general aspheric LSM optic, the surface equation may be obtained by requiring the optical path lengths to be constant for all axial rays passing through the entrance pupil and imaging at Z_I on the Z-axis. (See Shealy and Chao[15] for a more detailed discussion of constant optical path length methods).

RESULTS

Several spectral slicing x-ray telescopes utilizing the ATM Experiment S-056 Wolter I mirrors and the Stanford/MSFC Wolter-Schwarzschild mirrors as primaries have been designed and analyzed. The theoretical performance of these systems has been evaluated utilizing concave and convex spherical, concave ellipsoidal, convex hyperboloidal, and constant optical path aspheric LSM optics of 2X, 6X, and 8X magnifications. RMS blur circle radii and point spread functions have been calculated to evaluate the theoretical performance of each configuration. The analysis has been carried out for point sources on-axis and at off-axis field angles of 0.5, 1, 1.5, 2, 5, 10, and 16 arc minutes. The RMS blur circle radii for the spherical, ellipsoidal, and hyperboloidal LSM optics with S-056 are shown in Figures 5, 6, and 7. In Figure 8, the performance of the various LSM optics of magnification 2X is compared. It is seen that for the hyperboloidal, ellipsoidal, and aspherical LSM mirrors similar performance is predicted at all field angles, with the ellipsoidal element being slightly better at the edge of the field. The spherical element performs better than the others at the larger field angles, but is degraded near the axis due to spherical aberration.

Figure 9 presents the RMS versus field angle over the image plane located at the point of best focus for on-axis light for the S-056 with a convex spherical LSM. Comparing Figs. 5 and 9, one notes that the on-axis spherical aberration of the system is reduced by defocussing the image plane by .15 mm. Figure 10 presents the RMS versus field angle for S-056-convex spherical LSM when the image plane is defocussed + 1 mm from the point of best focus which displays typical defocussing errors.

The RMS vs. field angle for the nested Stanford/MSFC WS-convex spherical LSM is given in Fig. 11a for the Gaussian image plane location. Figure 12 presents the RMS vs. field angle for the nested Stanford/MSFC - convex spherical LSM with M=2 for when the image plane is defocussed by + 5 mils., which has little effect on reducing the on-axis spherical aberration of the system.

It should also be pointed out that since x-ray telescopes have sharply peaked point response functions, we have observed that spatial resolutions significantly better than the values obtained by RMS blur circle radii calculations are almost always achieved. In Table 2, more representative resolution values are given by the Full Width Half Maximum (FWHM) of the Point Spread Function (PSF) for spectral slicing x-ray telescopes at several field angles. From these results it can be seen that sub arc second performance should be realized over the entire field out to 16 arc minutes for the 2X mirrors. Even better performance is predicted for the 6X spherical optics.

Figures 13-17 present three-dimensional prospective plots of the point spread function of the S-056-convex spherical LSM for M=2, 6, 8 at different field angles. It can be seen that the sharp central peak remains well below 2 arc second in extent at all field angles. The results also illustrate the effect of varying the magnification on the resolution of the system. These are entirely optical effects, with no consideration given to detector characteristics. When these considerations are invoked, it is clear that better resolution will be achieved with the use of the higher power LSM mirrors. Of course, with a detector of fixed size, the use of a larger magnification will result in a smaller region of the Sun being imaged. Hence, the ability to shift from a low magnification, wide field image to a high magnification, high-resolution image of a selected

feature would have a tremendous value. Figures 18 and 19 present the FWHM of the meridional and sagittal section of the PSF for the S-056-convex spherical LSM system on the best focused flat focal plane. Sub-arc second resolution should be obtained over most of the field.

Figures 20-25 present the PSF for the nested Stanford/MSFC WS-convex spherical LSM over the best flat focal plane for M=2, 6, 8 and selected field angles. (Rays were traced only through half of the entrance pupil.) Figures 26-27 give the FWHM of the meridional and sagittal section of the PSF for the nested Stanford/MSFC WS-convex spherical LSM system rays are traced through half the entrance pupil. From these results, one concludes sub-arc second resolution should be obtained for a + 10 arc-min. field of view where the results in Figs. 26-27 have been doubled to determine resolution since only half of the entrance pupil was used during the ray trace.

The percent energy loss due to vignetting is shown in Fig. 28 for the S-056 based system and in Fig. 29 for the nested Stanford/MSFC WS based system.

In order to determine alignment tolerances for the LSM optics, a ray tracing analysis has been performed on the Spectral Slicing X-Ray system when the LSM element is (1) tilted while the vertex remains fixed on the optical axis as shown in Fig. 30 and (2) a line from the LSM vertex to center of curvature is displaced parallel to the optical axis as shown in Fig. 32. Figs. 30-31 present the RMS vs. tilt angle for the S-056 system, and Figs. 32-33 give the RMS vs. displacement distance. From these results, one concludes that a tilt angle of LSM with respect to the optical axis should be maintained to less than 0.1 degree and that a displacement of the LSM symmetry axis from the optical axis should be maintained to less than 0.1 mm. Figures 34-37 present the RMS vs. tilt

and decentration of the LSM for the nested Stanford/MSFC WS system. Similar alignment tolerance resulted for the nested WS system as obtained for the S-056 system.

CONCLUSION

Detailed theoretical design and analysis of several Spectral Slicing X-Ray Telescope systems using normal incidence LSM optics of various configurations and magnifications have been completed. It is shown that the spherical LSM optics should yield excellent (sub arc second) performance over the entire field. Ellipsoidal, hyperboloidal, and aspheric elements show better performance near the axis, but much of this advantage would not be relaized after the detector limitations are included. Hence, it has been concluded that the spherical LSM elements, which are far easier to fabricate and less costly, are preferred for the Spectral Slicing X-Ray Telescope Systems. Consequently, concave spherical LSM mirrors have been fabricated at Stanford University and are currently being subjected to visible light and x-ray tests at MSFC and Stanford. Some of these LSM optics will be flown on the MSFC/Stanford Wolter-Schwarzschild Telescope Rocket Experiment for high-resolution solar x-ray studies later this year.

REFERENCES

1. Wolter, H., Ann. Phys. 10, 94, 1952.

2. Wolter, H., Ann. Phys. 10, 286, 1952.

3. Schwarzschild, K., Abh. Ges. Wiss. Goettingen, Math.-Phys. Bd. IV, 1905.

4. Hoover, R. B., Thomas, R. J., and Underwood, J. H., Advances in Space Science and Technology 11, Academic Press, New York, 159, 1972.

5. Giacconi, R., et al., Ap. J. 230, 540, 1979.

6. Weisskopf, M.J., J. Wash. Acad. Sci. 71, (2), 69, 1981.

7. Underwood, J.H., Milligan, J.E., deLoach, A.C., and Hoover, R.B., Appl. Opt. 16, 858, 1977.

8. Chase, R.C., Davis, J.M., Kreiger, A.S., and Underwood, J.H., SPIE Proceedings 316, 74, 1981.

9. Shealy, D.L., Kassim, A., and Chao, S., Final Report on Contract NAS8-34728, submitted to George C. Marshall Space Flight Center, 1982.

10. Hoover, R.B., Cumings, N.P., Hildner, E., Moore, R.L., and Tandberg-Hanssen, E.A., NASA TM-86507, April 1985.

12. Underwood, J.H., Barbee, T.W., Jr., and Shealy, D.L., SPIE Proceedings 316, 79, 1981.

13. Spiller, E., Appl. Opt. 15, 2333, 1976.

14. Spiller, E., AIP Conference Proceedings75, 89, 1977.

15. Shealy, D.L. and Chao, S., Final Report on Contract NAS8-35916 submitted to George C. Marshall Space Flight Center, June 10, 1984.

16. Hoover, R.B., Chao, S.H., Shealy, D.L., SPIE Proceeding 563.39, 280-290, 1985.

APPENDIX A

Reprint of Ref. 16.

PROCEEDINGS
Of SPIE-The International Society for Optical Engineering

Volume 563

Applications of Thin-Film Multilayered Structures to Figured X-Ray Optics

Gerald F. Marshall
Chairman/Editor

Cooperating Organizations
Optical Sciences Center/University of Arizona
Institute of Optics/University of Rochester

August 20-22, 1985
San Diego, California

Design and analysis of spectral slicing x-ray telescope systems

Richard B. Hoover
Space Science Laboratory

George C. Marshall Space Flight Center
Marshall Space Flight Center, Alabama 35812

Shao-Hua Chao and David L. Shealy

Physics Department
University of Alabama at Birmingham
Birmingham, Alabama 35294

Abstract

Layered Synthetic Microstructure (LSM) x-ray optics can be used to couple a conventional Wolter Type I or Wolter-Schwarzschild x-ray mirror to a high sensitivity/broad wavelength response detector. Since the LSM mirror can effectively reflect only a narrow spectral slice of the incident radiation, this new instrument is referred to as a "Spectral Slicing X-Ray Telescope." By the use of figured multilayer (LSM) optics, it is possible to alter the plate scale of the primary mirrors to allow improved spatial resolution to be realized with solid state detectors.

We will present the results of theoretical design and analysis studies of several spectral slicing x-ray telescope systems utilizing LSMs figured as hyperboloids, spheres, ellipsoids, and constant optical path aspheric elements. The RMS spot size and point spread function calculations will be presented for systems in which the LSM optics are figured to yield magnifications of 2X, 6X, and 8X, and it will be demonstrated that these systems yield superior off-axis performance over the primary optic alone.

Introduction

Over the past two decades, numerous glancing incidence x-ray telescopes have been fabricated and flown on sounding rockets and satellites to produce high-resolution images of the Sun and cosmic x-ray sources. The optics for these telescopes usually involve conic surfaces of revolution, which were first described by H. Wolter[1] in 1952 as systems for aplanatic x-ray microscopes. Subsequently, Wolter[2] modified the Schwarzschild[3] general equations for two-element reflecting telescopes. These Wolter-Schwarzschild systems generally yield slightly improved performance at the larger field angles, but the mirrors are more complex and difficult to fabricate. Wolter Type II mirrors use an internally reflecting paraboloid followed by an externally reflecting hyperboloid (Figure 1b). This system has found wide applications in XUV/EUV astronomy where the primary interest is in the wavelength range greater than 100 Å. Wolter Type I optics (Figure 1a), where the internally reflecting paraboloid is followed by an internally reflecting hyperboloid, has been the most extensively used imaging system for x-ray telescopes designed to operate in the 3 - 100 Å region. (See Hoover, Thomas, and Underwood[4] for a general review of the principles of glancing incidence x-ray optics.) Nested Wolter I mirrors were utilized on the Einstein Observatory[5] (which revolutionized cosmic x-ray astronomy) and are being planned for the Advanced X-Ray Astrophysics Facility (AXAF).[6]

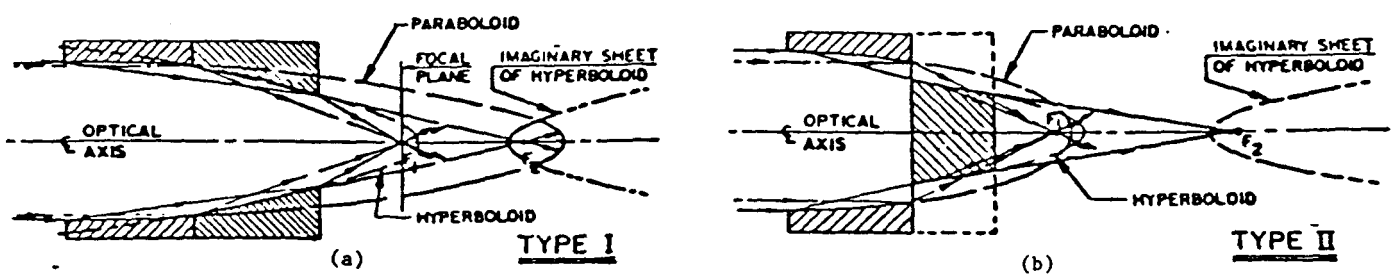

Figure 1. Optical configuration of (a) Wolter Type I and (b) Wolter Type II glancing incidence x-ray telescopes.

Our knowledge of solar x-ray phenomena was dramatically increased in 1973 by Wolter I telescopes carried aboard the Apollo Telescope Mount (ATM) on the Skylab mission. During this mission, ATM experiments S-056 (MSFC) and S-054 (American Science & Engineering) produced over 70,000 high-resolution x-ray images that provided a wealth of information regarding solar flares, coronal holes, and x-ray bright points. Both of these telescopes employed photographic emulsions as x-ray detectors, and the film magazines were removed by the astronauts and returned to Earth for processing and analysis. While photographic emulsions afford higher spatial resolution than can be presently obtained with solid state detectors such as CCD's, film has a much lower sensitivity. Film also has the disadvantage that it must be retrieved and developed before analysis. This makes film an unsuitable detector for use on many unmanned satellites and observatories.

It is now well established that glancing incidence Wolter I x-ray telescopes have a sharply peaked point response function and that the spatial resolution realized with these systems is in general limited by the detector. For example, solar x-ray images recorded by ATM Experiment S-056 with a 1.9 m focal length (plate scale 9 μm/arc second) exhibited a resolution limit of 2.2 arc seconds on SO-212 film (uncoated Panatomic-X) and 1.8 arc seconds on SO-242 film. However, in laboratory tests using Kodak High-Resolution Photographic Plates, spatial resolution of 0.75-0.8 arc seconds was achieved with these flight optics.[7] Hence, limitations of the spatial resolution imposed even by high-resolution detectors such as film may degrade the performance of state-of-the-art x-ray telescopes. Far more severe degradations would be experienced with solid state detectors, which afford much higher sensitivity over broader spectral ranges but currently have lower spatial resolution than can be achieved with photogrphic film. Technological limitations presently make it impossible to fabricate solid state detectors with pixel sizes much smaller than 10 μm. Better resolution with these devices can be realized with telescopes of longer focal length and therefore increased plate scale. However, these instruments are of necessity heavier and more costly, and may exceed the envelopes allowed by some sounding rockets and satellites.

For these reasons, various techniques for using auxiliary optics to increase the plate scale without significantly increasing the telescope physical length have been studied. Chase et al.[8] investigated Grazing Incidence Relay Optics (GIRO) as a means of coupling x-ray mirror systems to detectors. In the MSFC Extended Range X-Ray Telescope (ERXRT) program, several glancing incidence hyperboloid/ellipsoid x-ray microscope optics of different magnifications and focal lengths were designed and analyzed.[9,10] The studies optimized an x-ray microscope optic (8X) for use in coupling the ATM Experiment S-056 x-ray optics to a CCD of 30 μm pixel size. The ERXRT with a 4-meter telescope possesses a plate scale that would normally require an instrument 16 meters long. Ray trace results indicate that sub arc second performance should be achievable over the entire 4 arc minute field-of-view afforded by the 320X512 x-ray sensitive area of the RCA CCD. Since the microscope optics can be configured to operate at glancing angles similar to the primary, it is possible to reflect x-rays over the entire spectral range covered by the Wolter x-ray optics. Although x-ray microscope optics are expensive and difficult to fabricate and the image quality and throughput degrades fairly rapidly with field angle, these optics should be of great value for high-resolution imaging of selected features over broad spectral ranges and for use in conjunction with high-resolution x-ray spectrometers.

An alternative system for realizing the high inherent resolution capability of the Wolter optics without significantly increasing the telescope physical length should be achieved by the use of Layered Synthetic Microstucture (LSM) optics.[11-14] As determined by the optical properties and thickness of the multilayers, the LSMs can be tailored to reflect only specific narrow spectral slices of the incident x-ray beam. By the use of normal incidence LSM optics on properly contoured substrates, spectral slicing x-ray telescope systems with variable magnifications may be realized (Figure 2). Variable magnification would allow the instrument to shift from moderate resolution x-ray images of the entire solar disk to very high-resolution images of selected active regions, loops, bright points, or other features of interest. The narrow bandpasses afforded by properly designed LSM optics should permit far superior plasma diagnostics to be performed than was possible from the crude filtergrams obtained during the Skylab mission. Since it is unnecessary to increase the physical length of the instrument, these systems should be ideal for sounding rockets and many satellites that have limitations with regard to the size of payload that can be accommodated.

Presented herein are the results of our theoretical investigations of spectral slicing x-ray telescope systems in which the ATM Experiment S-056 Wolter I optics and the nested Wolter-Schwarzschild mirrors from the Stanford/MSFC Rocket Experiment are considered as the primary optics. The basic optical parameters for these mirrors are presented in Table 1. The performance of these systems was evaluated for LSM optics of hyperboloidal, spherical, ellipsoidal, and constant optical path aspheric configurations. We have calculated the RMS blur circle radii, the point response functions, and the full width half maxima of the line spread functions to establish the resolution theoretically attainable. The percent energy loss as a function of field angle was also established by ray trace procedures.

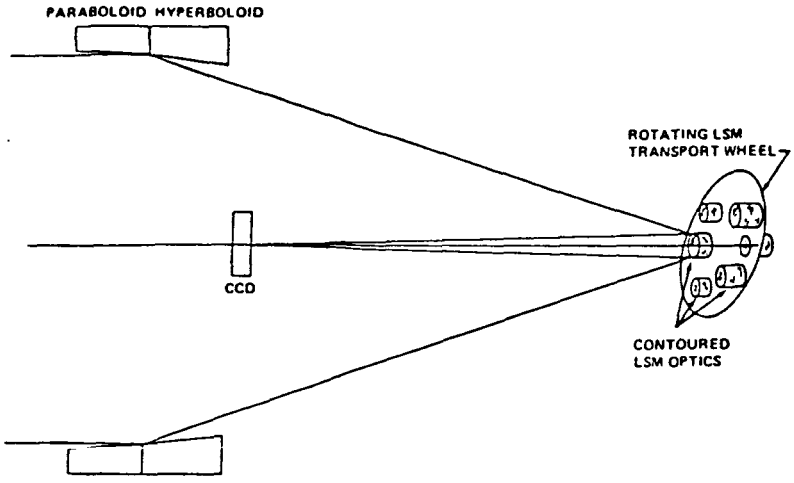

Figure 2. Schematic of Spectral Slicing X-Ray Telescope.

Table 1. Primary Mirror Parameters

S-056 Wolter I		Wolter-Schwarzschild	
Focal Length	190.5 cm	Focal Length	128.2 cm
Glancing Angle	0.916°	Glancing Angle	2.0° (outer mirror)
			1.7° (inner mirror)
z_p max	392.76 cm		
z_p min	380.62 cm	Inner Diameter	
z_h min	369.19 cm	at Aperture	37.4 cm (outer mirror)
r_p max	12.36 cm		33.0 cm (inner mirror)
r_p min	12.17 cm	Element Lengths	26.7 cm (primary)
A	95.02 cm		21.8 cm (secondary)
B	4.31 cm	Collecting Area	107 cm^2 (outer mirror)
C	95.25 cm		80 cm^2 (inner mirror)
P	0.1946 cm		
Collecting Area	14.6 cm^2		

Mathmatical Analysis of the Spectral Slicing X-Ray Telescope

The Spectral Slicing X-Ray Telescope is based upon the concept of using normal incidence contoured LSM optics to reflect and magnify a narrow spectral slice of the x-ray image produced by the primary mirrors. As is seen in Figure 3, this can be accomplished by means of either convex LSM mirrors placed in front of the prime focus or concave LSM optics behind the focus. The x-rays are reflected by the LSM optics to form a magnified image on the detector located at z_I on the Z-axis. The design condition requires that an on-axis incident ray that strikes the intersection (R_2,Z_2) of the primary Wolter optics be reflected by the LSM optics to form an image at the detector. The geometry of the Spectral Slicing X-Ray Telescope is shown in Figure 4. The surface parameters of the LSM optics are determined by the design condition and the LSM surface equation. The results are expressed in terms of the magnification of the LSM mirror:

$$M = -v/u, \tag{1}$$

where u and v are the object and image distances shown in Figure 4. They are given by:

$$u = z_{03} - \bar{z} \tag{1a}$$

$$-v = z_I - z_{03} \tag{1b}$$

The axial ray intercept, $\bar{z}$, of ray reflected from the Wolter optics is evaluated from the ray trace equation:

$$\bar{z} = z_2 - x_2 A_{2z}/A_{2x} \quad , \tag{2}$$

where A_{2x}, A_{2z} are the x,z direction cosines for the ray reflected from the point (X_2,Z_2) on the Wolter telescope.

For a convex spherical LSM optic, the surface equation is given by:

$$(z_3 - z_{03} + R_3)^2 + x_3^2 + y_3^2 = R_3^2 \quad , \tag{3}$$

where z_{03} is the surface vertex and R_3 is the radius of curvature of the LSM.

Solving Equations 1 and 2 for z_{03} gives:

$$z_{03} = \frac{z_I + \bar{z}M}{1 + M} \quad . \tag{4}$$

R_3 is obtained from the paraxial mirror equation by requiring an image to be produced at the detector:

$$\frac{1}{u} + \frac{1}{v} = \frac{-2}{R_3} \quad . \tag{5}$$

Solving equations 1-5 gives:

$$R_3 = \frac{2M(\bar{z} - z_I)}{M^2 - 1} \quad . \tag{6}$$

Numerical values for R_3 and z_{03} for the configuration of the S-056 primary with a convex LSM spherical optics are as follows.

M	R_3 (cm)	z_{03} (cm)
2	269.94	257.88
6	69.37	219.37
8	51.38	212.95

The Wolter-Schwarzschild/convex sperical LSM values are:

M	R_3 (cm)	z_{03} (cm)
2	204.89	51.22
6	52.88	22.03
8	39.71	17.37

For a concave ellipsoidal LSM mirror, the surface equation is given by:

$$\frac{(z_3 - z_I - C_E)^2}{A_E^2} + \frac{R_3^2}{B_E^2} = 1 \quad , \tag{7}$$

where A_E, B_E, and C_E are the surface parameters determined by requiring that one of the foci be at $\bar{z}$ and the other be at z_I on the Z-axis. The mirror surface parameters satisfy the following equations:

$$A_E = C_E \frac{(1 + M)}{M - 1} \quad , \tag{8}$$

$$B_E^2 = A_E^2 - C_E^2 \quad , \tag{9}$$

$$C_E = \frac{1}{2} (z_I - \bar{z}) \quad , \tag{10}$$

and the values for the S-056 concave ellipsoidal LSM optics for magnifications of 2X, 6X, and 8X are given below.

M	A_E (cm)	B_E (cm)	C_E (cm)
2	303.38	286.02	101.12
6	141.57	99.08	101.12
8	130.01	81.72	101.12

For a convex hyperboloidal LSM optic, the surface equation is given by:

$$\frac{(z_3 - z_I - C_H)^2}{A_H^2} - \frac{R_3^2}{B_H^2} = 1 \tag{11}$$

where A_H, B_H, and C_H are the surface parameters of the hyperboloid as determined by the requirement that one of the foci be at $\bar{z}$ and the other be at z_I on the Z-axis. These surface parameters are given by:

$$A_H = C_H \frac{(M - 1)}{(M + 1)} \quad , \tag{12}$$

$$B_H^2 = C_H^2 - A_H^2 \quad , \tag{13}$$

$$C_H = \frac{(z_I - \bar{z})}{2} \quad , \tag{14}$$

and their numerical values for the S-056/convex hyperboloidal LSM are as follows:

M	A_H (cm)	B_H (cm)	C_H (cm)
2	33.70	95.34	101.12
6	72.23	70.77	101.12
8	78.65	63.56	101.12

For a general aspheric LSM optic, the surface equation may be obtained by requiring the optical path lengths to be constant for all axial rays passing through the entrance pupil and imaging at z_I on the Z-axis. (See Shealy and Chao[15] for a more detailed discussion of constant optical path length methods.)

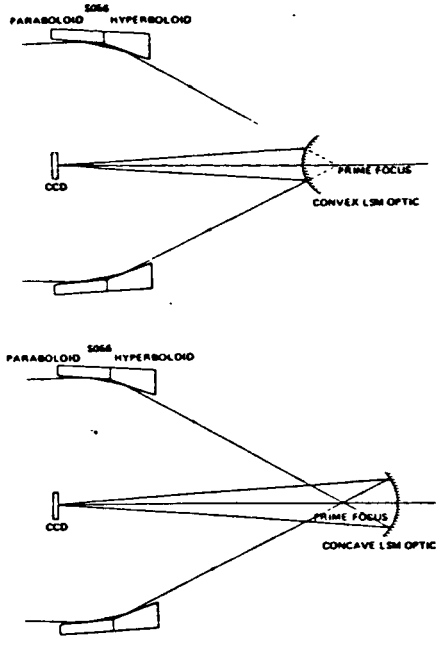

Figure 3. Convex and concave LSM optics with S-056 primary.

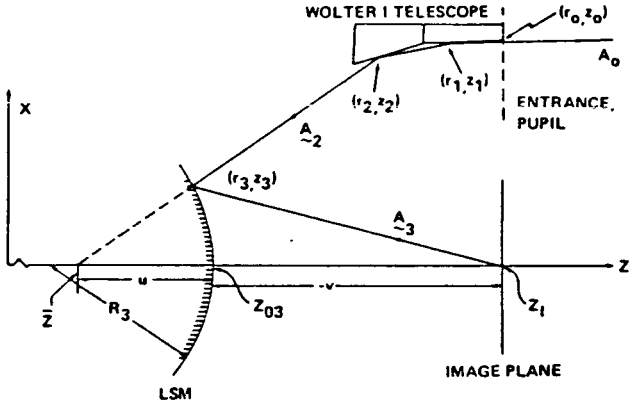

Figure 4. Geometry of Spectral Slicing X-Ray Telescope.

Results

Several spectral slicing x-ray telescopes utilizing the ATM Experiment S-056 Wolter I mirrors and the Stanford/MSFC Wolter-Schwarzschild mirrors as primaries have been designed and analyzed. We have calculated the theoretical performance of these systems utilizing concave and convex spherical, concave ellipsoidal, convex hyperboloidal, and constant optical path aspheric LSM optics of 2X, 6X, and 8X magnifications. RMS blur circle radii and point spread functions have been calculated to evaluate the theoretical performance of each configuration. The analysis has been carried out for point sources on-axis and at off-axis field angles of 0.5, 1, 1.5, 2, 5, 10, and 16 arc minutes. The RMS blur circle radii for the spherical, ellipsoidal, and hyperboloidal LSM optics with S-056 are shown in Figures 5, 6, and 7. In Figure 8, the performance of the various LSM optics of magnification 2X is compared. It is seen that for the hyperboloidal, ellipsoidal, and aspherical LSM mirrors similar performance is predicted at all field angles, with the ellipsoidal element being slightly better at the edge of the field. The spherical element performs better than the others at the larger field angles, but is degraded near the axis due to spherical aberration.

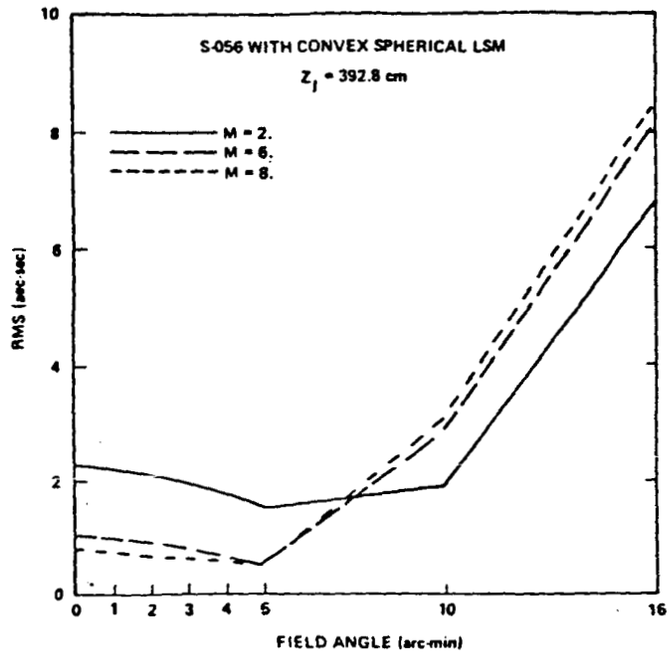

Figure 5. RMS blur circle radius as a function of field angle and magnification for a Spectral Slicing X-Ray Telescope with a Wolter I primary and convex spherical LSM. (Gaussian focal plane.)

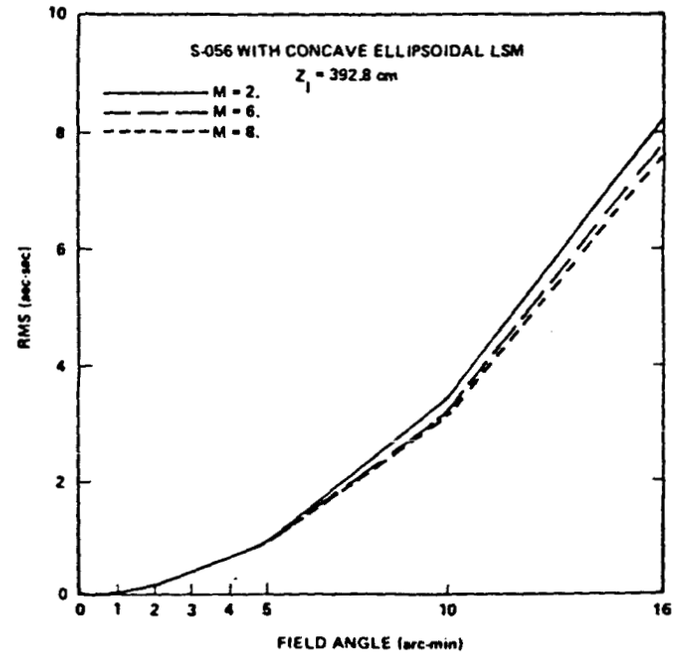

Figure 6. RMS blur circle radius as a function of field angle and magnification for a Spectral Slicing X-Ray Telescope with a Wolter I primary and concave ellipsoidal LSM. (Gaussian focal plane.)

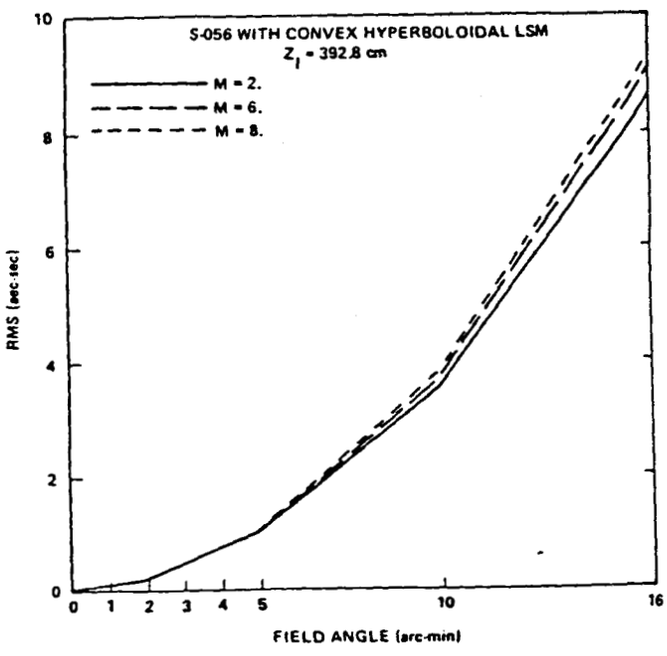

Figure 7. RMS blur circle radius as a function of field angle and magnification for a Spectral Slicing X-Ray Telescope with a Wolter I primary and convex hyperboloidal LSM. (Gaussian focal plane.)

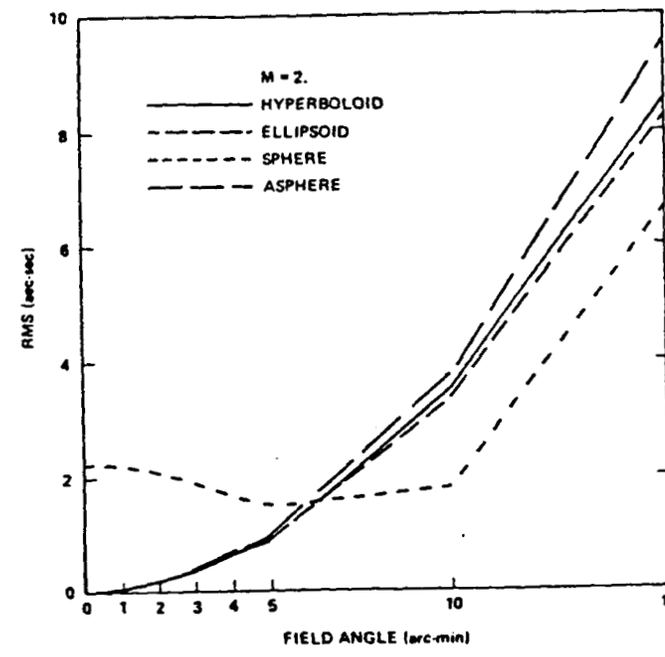

Figure 8. RMS blur circle radius as a function of field angle for magnification 2X LSM optics of different contours with S-056 primary. (Gaussian focal plane.)

It should also be pointed out that since x-ray telescopes have sharply peaked point response functions, we have observed that spatial resolutions significantly better than the values obtained by RMS blur circle radii calculations are almost always achieved. In Table 2, more representative resolution values are given by the Full Width Half Maximum (FWHM) of the Point Spread Function (PSF) for spectral slicing x-ray telescopes at several field angles. From these results it can be seen that sub arc second performance should be realized over the entire field out to 16 arc minutes for the 2X mirrors. Even better performance is predicted for the 6X spherical optics.

Table 2. Spectral Slicing X-Ray Telescope Systems (S-056)

LSM Optics	Field Angle (arc min)	FWHM (arc sec)* Meridional	Sagittal
SPHERICAL M = 2	on-axis	0.61	0.61
	1	0.59	0.59
	5	0.40	0.45
	10	0.16	0.21
	16	0.43	0.68
ELLIPSOIDAL M = 2	on-axis	0.00	0.00
	1	0.004	0.004
	5	0.13	0.14
	10	0.58	0.59
	16	1.02	1.83
HYPERBOLOIDAL M = 2	on-axis	0.00	0.00
	1	0.004	0.005
	5	0.142	0.142
SPHERICAL M = 6	on-axis	0.24	0.24
	1	0.25	0.24
	5	0.035	0.055

*Full Width Half Maximum on Gaussian focal plane.

In Figure 9 we present three-dimensional perspective plots of the point spread function of S-056 with a 2X spherical LSM at field angles of 5, 10, and 16 arc minutes. It can be seen that the sharp central peak remains well below 1 arc second in extent at all field angles. Figure 10 illustrates the effect of varying the magnification on the resolution of the system. These are entirely optical effects, with no consideration given to detector characteristics. When these considerations are invoked, it is clear that better resolution will be achieved with the use of the higher power LSM mirrors. Of course, with a detector of fixed size, the use of a larger magnification will result in a smaller region of the Sun being imaged. Hence, the ability to shift from a low magnification, wide field image to a high magnification, high-resolution image of a selected feature would have a tremendous value.

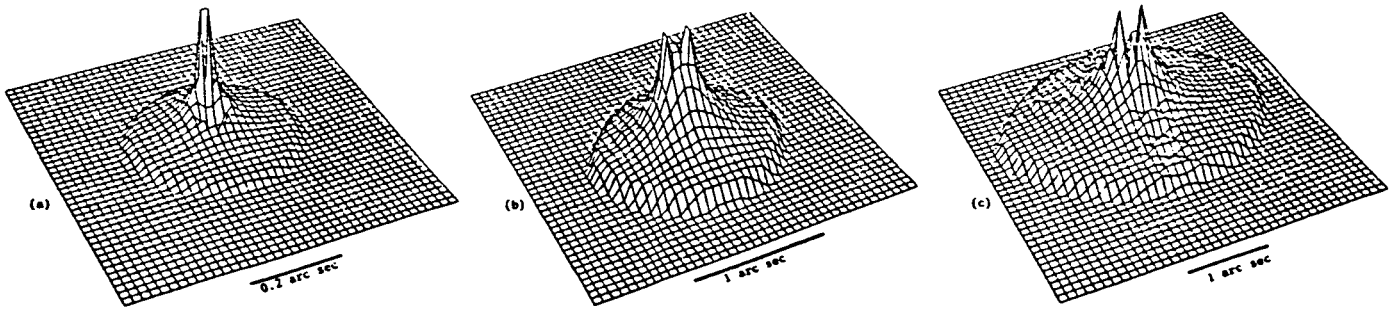

Figure 9. Three-dimensional perspective plots of the point spread function for a Spectral Slicing X-Ray Telescope with a 2X spherical LSM at field angles of (a) 5 arc minutes, (b) 10 arc minutes, and (c) 16 arc minutes, on best flat focal plane ($\Delta Z = \pm .15$ cm)

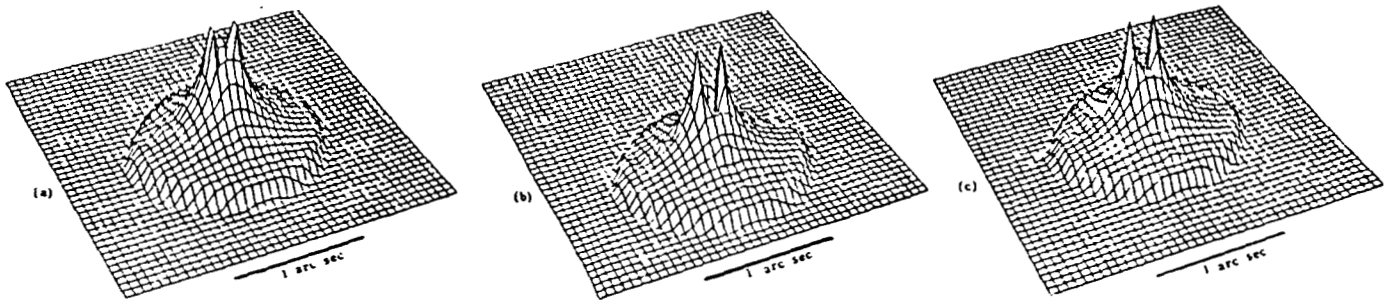

Figure 10. Three-dimensional perspective plots of the point spread function on the best flat focal plane at a field angle of 10 arc minutes with spherical LSM optics affording magnifications of (a) 2X (ΔZ = -.15 cm) (b) 6X (ΔZ = -.59 cm) and (c) 8X (ΔZ = -.8 cm).

The use of contoured LSM optics in conjunction with the nested Wolter-Schwarzschild mirrors has also been investigated. Figures 11 and 12 show the meridional and sagittal line spread functions for this system with convex spherical LSM optics for magnifications of 2X, 6X, and 8X. Excellent performance over the entire field is predicted. The percent energy loss is shown in Figure 13. Due to effects of the nested primary, it is not linear, but it remains at a very low value (less than 16%) over the entire field. The percent energy loss for S-056 with convex spherical LSM optics is presented in Figure 14. It is found to be linear with field angle and independent of magnification. The effects of decentering, tilting, and defocussing the LSM optics have also been studied and the results will be presented elsewhere.

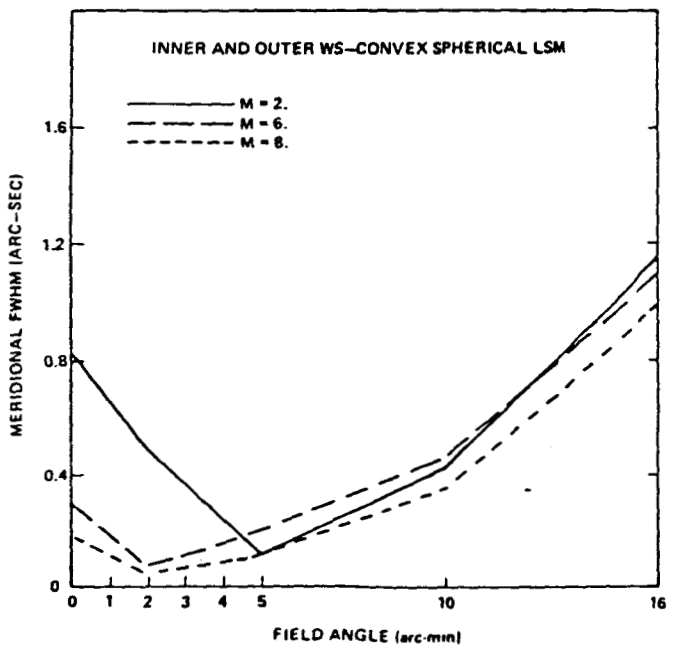

Figure 11. Meridional line spread function (FWHM) as a function of field angle for Wolter-Schwarzschild mirrors with convex spherical LSM. (Gaussian focal plane).

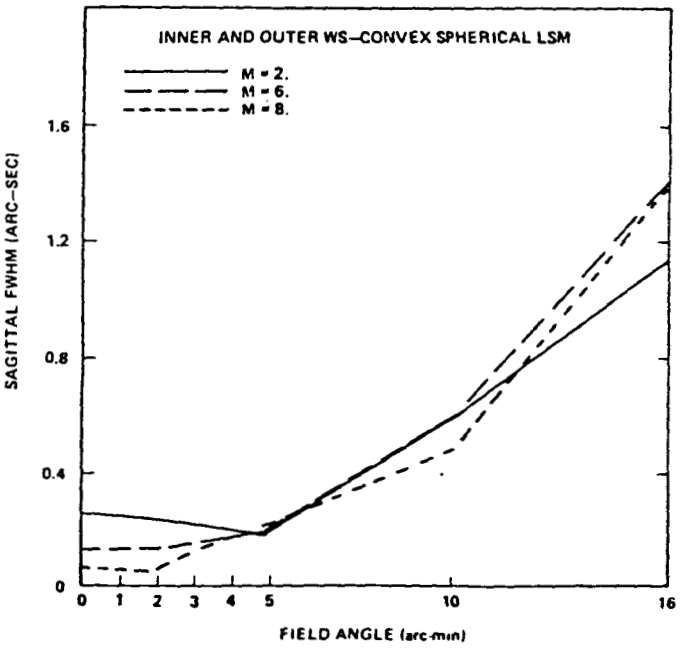

Figure 12. Sagittal line spread function (FWHM) as a function of field angle for Wolter-Schwarzschild mirrors with convex spherical LSM. (Gaussian focal plane.)

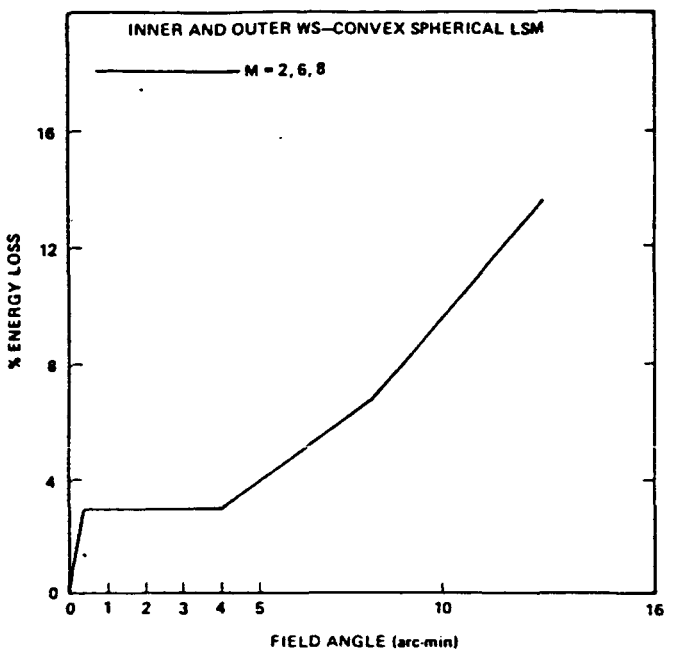

Figure 13. Percent energy loss for Spectral Slicing X-Ray Telescope with nested Wolter-Schwarzschild primary. (Gaussian focal plane).

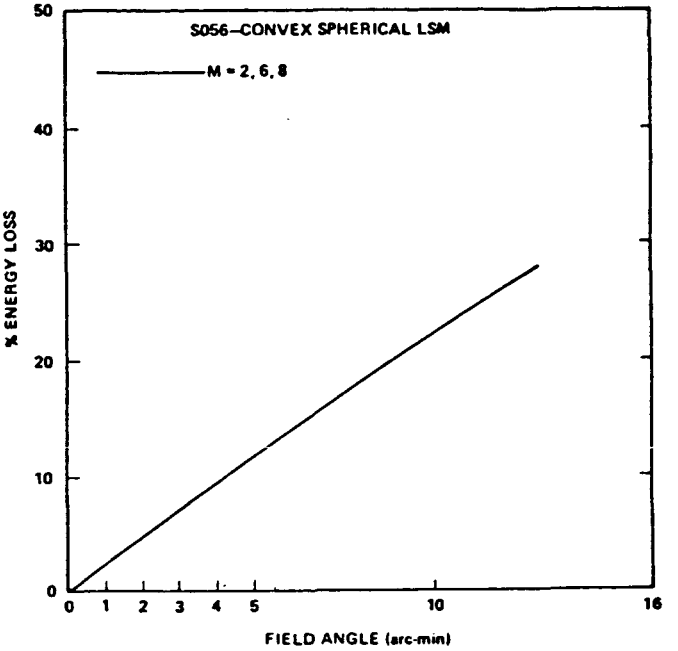

Figure 14. Percent energy loss for Spectral Slicing X-Ray Telescope with S-056 primary. (Gaussian focal plane).

Perhaps the most exciting result to be reported is the fact that LSM optics should not only allow the image to be magnified for better utilization with state-of-the-art solid state detectors, but it also exhibits the ability to improve the imaging properties of the primary Wolter I mirror system. By comparing the point spread functions for the S-056/spherical LSM, as shown in Figure 9, with those for S-056 alone (see Ref. 4, p. 175), one concludes that the resolution of the Spectral Slicing Telescope is improved by almost a factor of 2 at the larger field angles. This effect is due to a reduction in the optical aberrations (including the offense against the Abbé Sine Condition) of the entire system.

Conclusions

Detailed theoretical design and analysis of several Spectral Slicing X-Ray Telescope systems using normal incidence LSM optics of various configurations and magnifications have been completed. It is shown that the spherical LSM optics should yield excellent (sub arc second) performance over the entire field. Ellipsoidal, hyperboloidal, and aspheric elements show better performance near the axis, but much of this advantage would not be realized after the detector limitations are included. Hence, it has been concluded that the spherical LSM elements, which are far easier to fabricate and less costly, are preferred for the Spectral Slicing X-Ray Telescope systems. Consequently, concave spherical LSM mirrors have been fabricated at Stanford University and are currently being subjected to visible light and x-ray tests at MSFC and Stanford. Some of these LSM optics will be flown on the MSFC/Stanford Wolter-Schwarzschild Telescope Rocket Experiment for high-resolution solar x-ray studies later this year.

Acknowledgments

The authors wish to acknowledge the support of Dr. Fred Speer and the MSFC Center Director's Discretionary Fund Program which made this work possible.

References

1. Wolter, H., Ann. Phys. 10, 94, 1952.
2. Wolter, H., Ann. Phys. 10, 286, 1952.
3. Schwarzschild, K., Abh. Ges. Wiss. Goettingen, Math.-Phys. Bd. IV, 1905.
4. Hoover, R. B., Thomas, R. J., and Underwood, J. H., Advances in Space Science and Technology 11, Academic Press, New York, 159, 1972.
5. Giacconi, R., et al., Ap. J. 230, 540, 1979.
6. Weisskopf, M. J., J. Wash. Acad. Sci. 71(2), 69, 1981.

7. Underwood, J. H., Milligan, J. E., deLoach, A. C., and Hoover, R. B., Appl. Opt. 16, 858, 1977.
8. Chase, R. C., Davis, J. M., Kreiger, A. S., and Underwood, J. H., SPIE Proceedings 316, 74, 1981.
9. Shealy, D. L., Kassim, A., and Chao, S., Final Report on Contract NAS8-34728, submitted to George C. Marshall Space Flight Center, 1982.
10. Hoover, R. B., Cumings, N. P., Hildner, E., Moore R. L., and Tandberg-Hanssen, E. A., NASA TM-86507, April 1985.
11. Underwood, J. H., Barbee, T. W., Jr., and Keith, D. C., SPIE Proceedings 184, 123, 1979.
12. Underwood, J. H., Barbee, T. W., Jr., and Shealy, D. L., SPIE Proceedings 316, 79, 1981.
13. Spiller, E., Appl. Opt. 15, 2333, 1976.
14. Spiller, E., AIP Conference Proceedings 75, 89, 1977.
15. Shealy, D. L. and Chao, S., Final Report on Contract NAS8-35916 submitted to George G. Marshall Space Flight Center, June 10, 1984.

APPENDIX B

Contract Work Statement

Theoretical Analysis of Wolter/LSM X-Ray Telescope Systems

Scope of Work

I. Perform Ray Trace Analysis of the Spectral Slicing Zoom X-Ray Telescope System for configurations in which a convex LSM optic is placed in front of the prime focus or a concave LSM optic is placed behind the prime focus. The analysis will consider, hyperboloids, spheres, ellipsoids and constant optical path aspheric elements for two configurations:

A. The ATM Experiment S-056 Wolter I mirrors constitute the primary optics.

B. The Stanford/MSFC Rocket Wolter-Schwarzchild mirrors constitute the primary optics.

For both configurations, the PSF will be calculated for a point source on-axis and off-axis at the following field anges: 0.5 min; 1 min; 1.5 min; 2 min, 5 min; 10 min; and 16 min. The point response functions for both the meridional and sagittal planes will be generated. These data will be presented numerically and with 2- and 3-dimensional plot representations for the selected field angles.

II. The RMS Blur Circle radius for flat and optimally curved detector surfaces will be calculated to evaluate the effects of de-focussing for mirrors of magnifications of 2X, 6X, or 8X.

III. The effects of de-centration and tilt of the selected LSM's upon performance of the system will be carried out to determine mounting and alignment tolerances.

IV. The vendor will evaluate vignetting effects and LSM aperture requirements.

V. Critical mirror parameters required for fabrication for the selected LSM optics will be generated and provided to the PI.

VI. Vendor will provide interim data to the MSFC Principal Investigator.

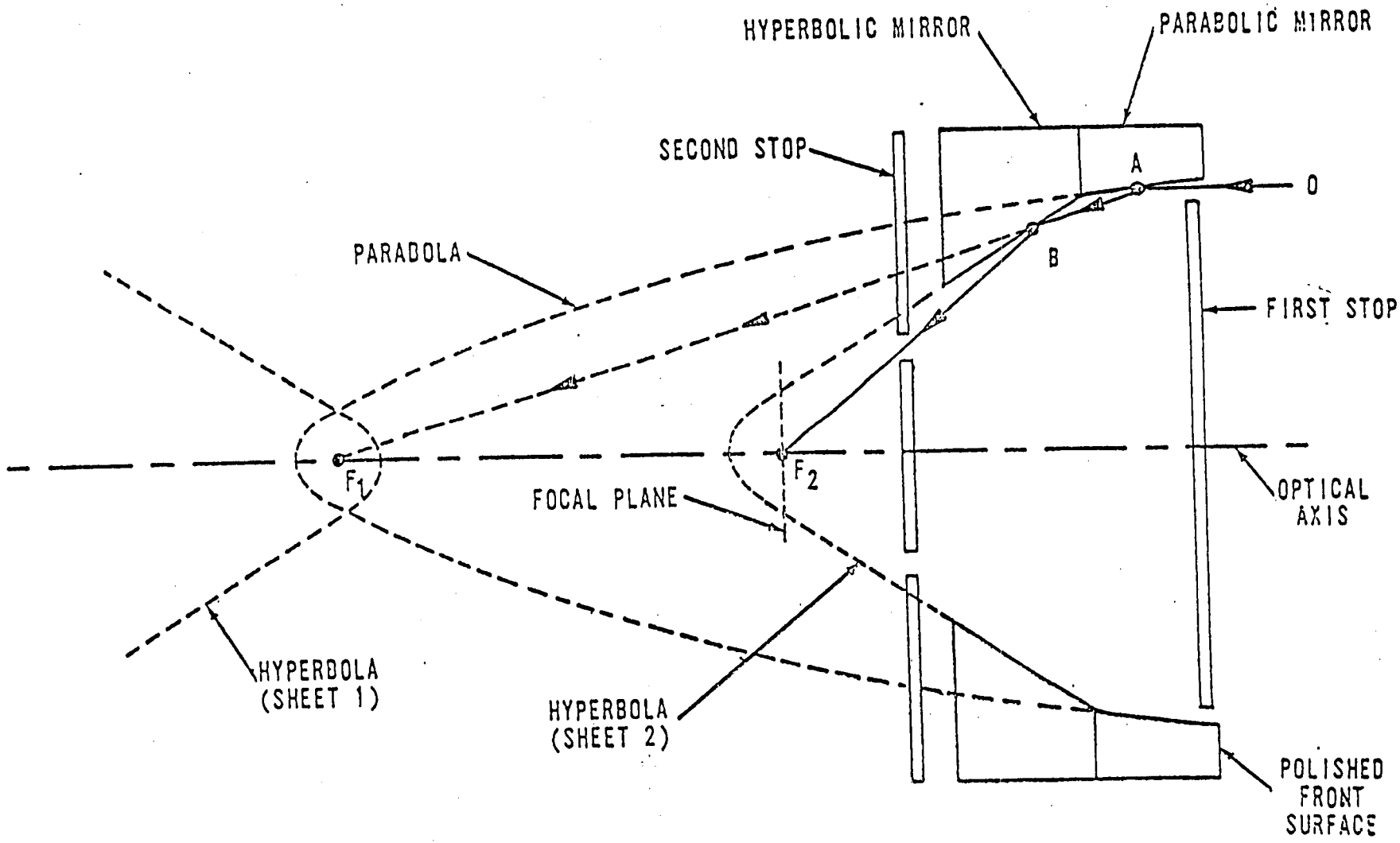

Fig. 1. Wolter I X-Ray Telescope Configuration.

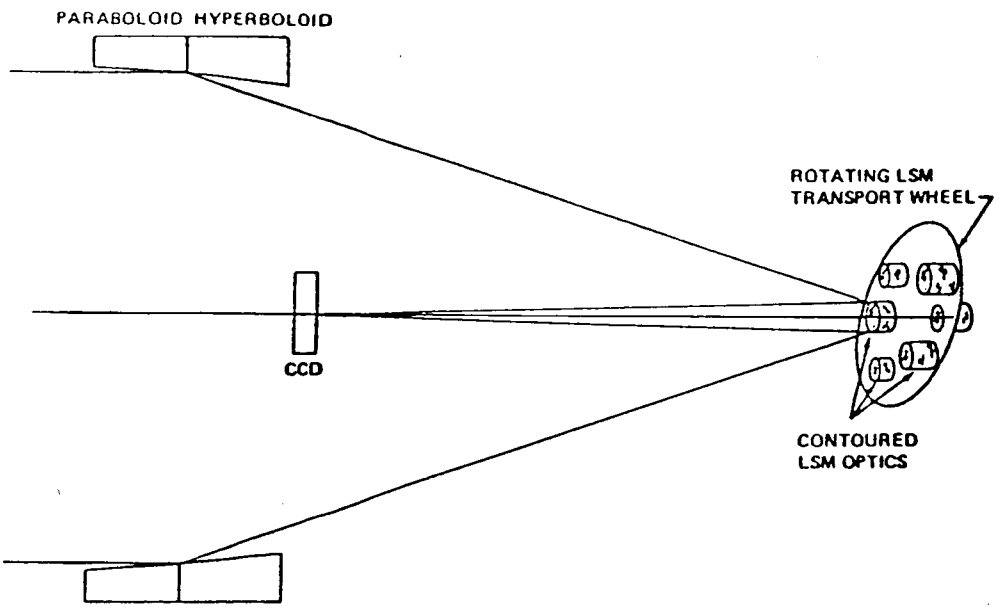

Figure 2. Schematic of Spectral Slicing X-Ray Telescope.

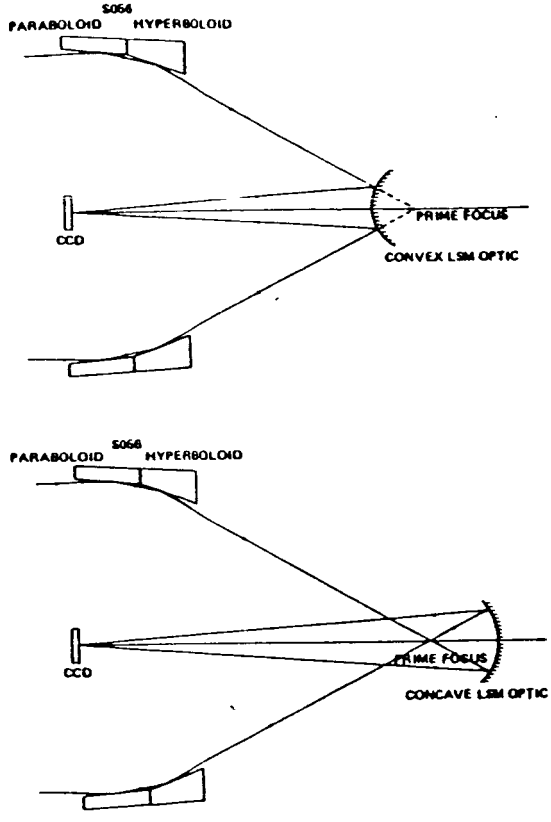

Figure 3. Convex and concave LSM optics with S-056 primary.

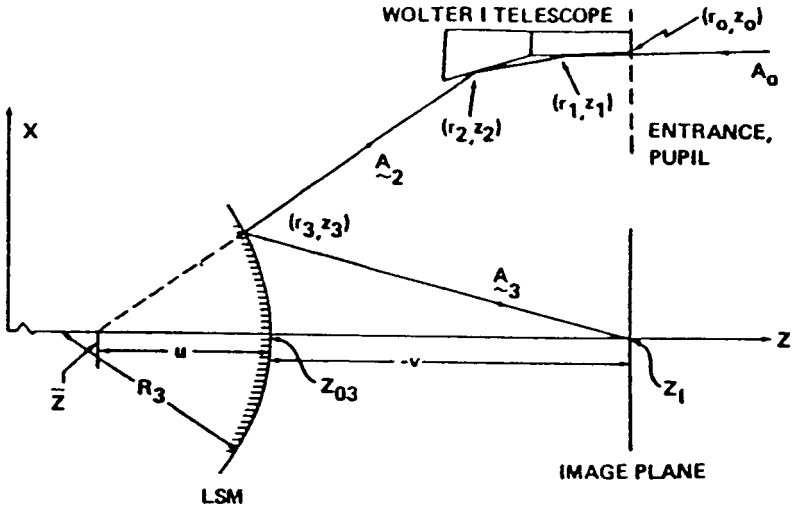

Figure 4. Geometry of Spectral Slicing X-Ray Telescope.

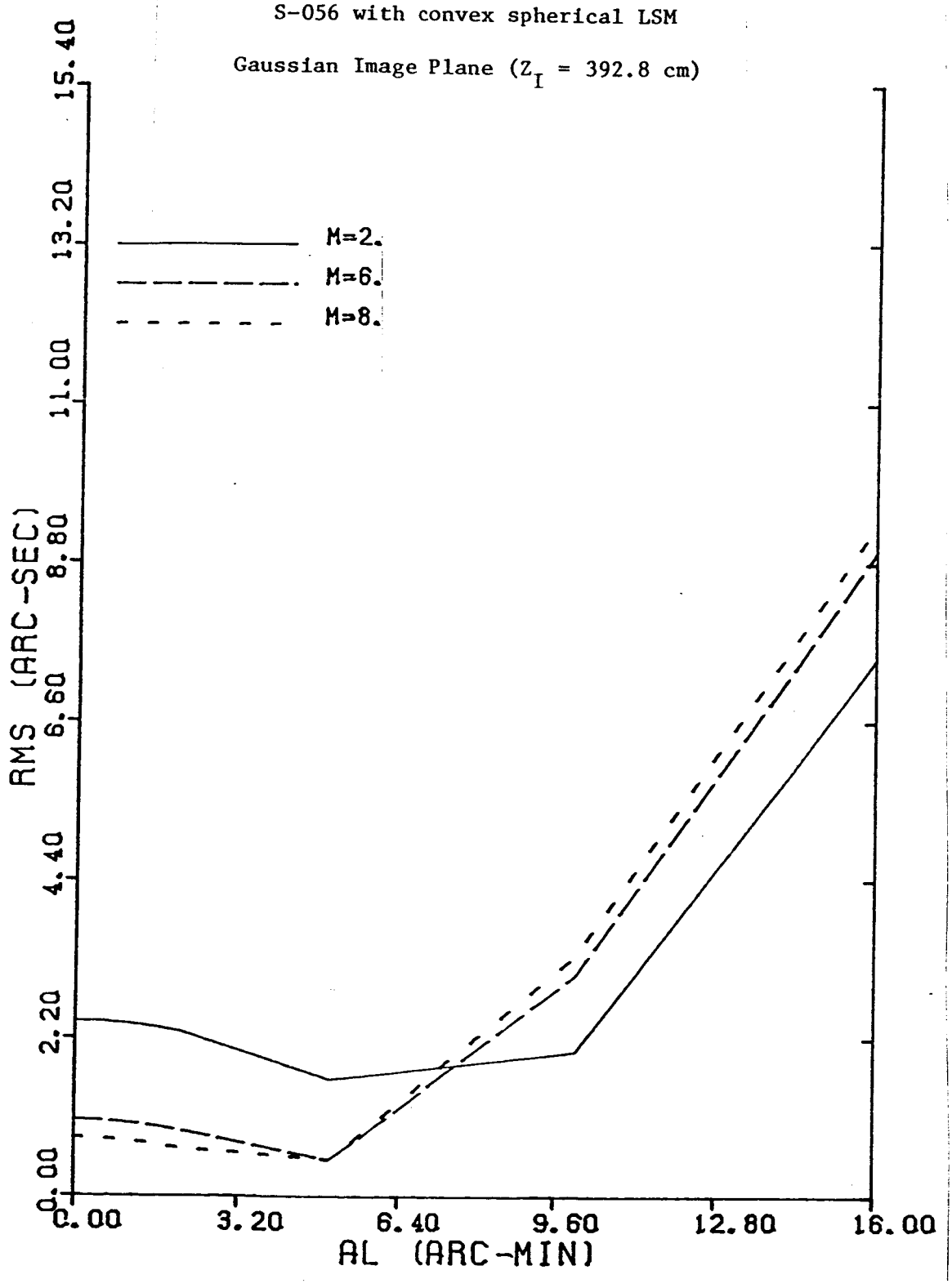

Figure 5. RMS blur circle radius as a function of field angle and magnification for a Spectral Slicing X-Ray Telescope with a Wolter I primary and convex spherical LSM.

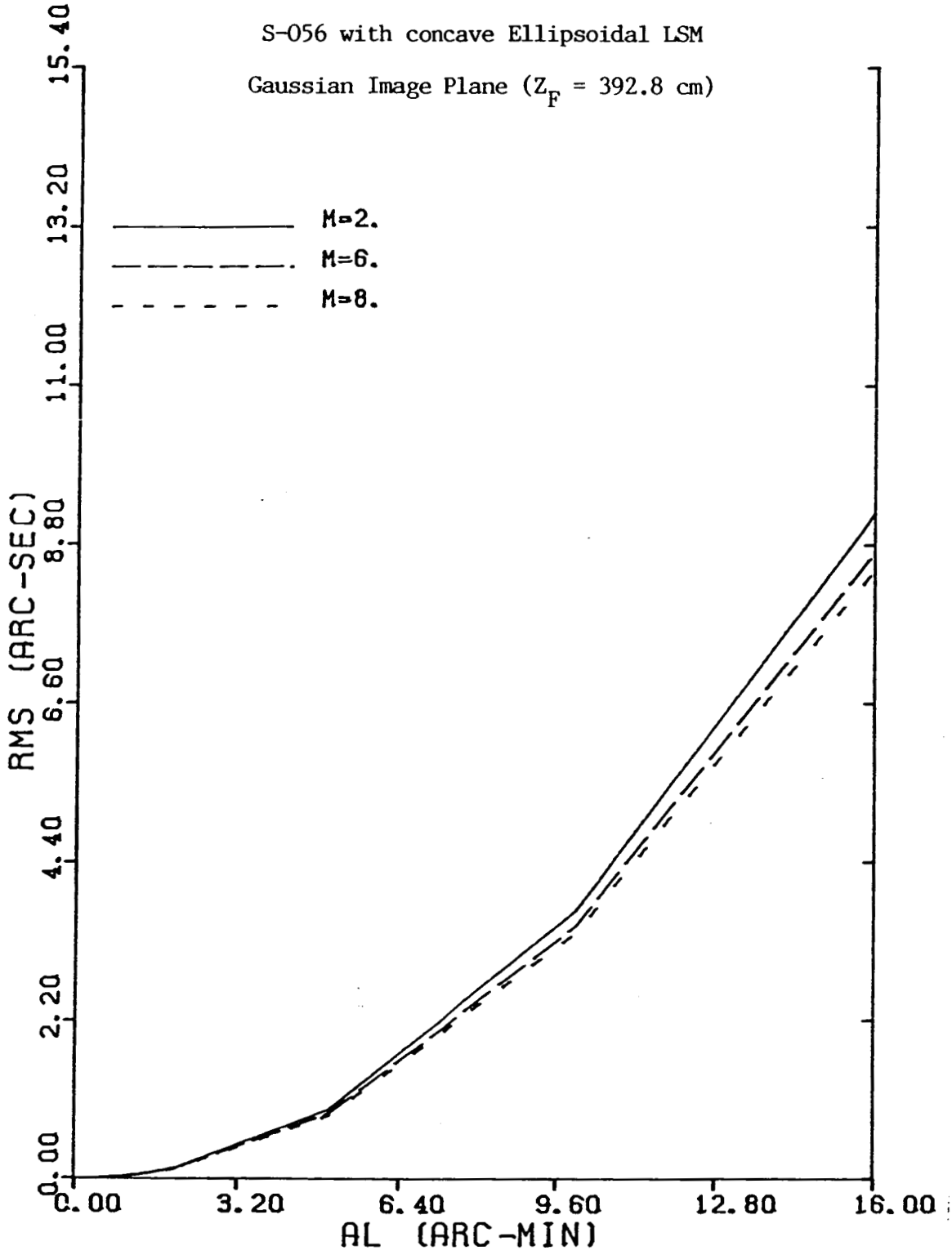

Figure 6. RMS blur circle radius as a function of field angle and magnification for a Spectral Slicing X-Ray Telescope with a Wolter I primary and concave ellipsoidal LSM.

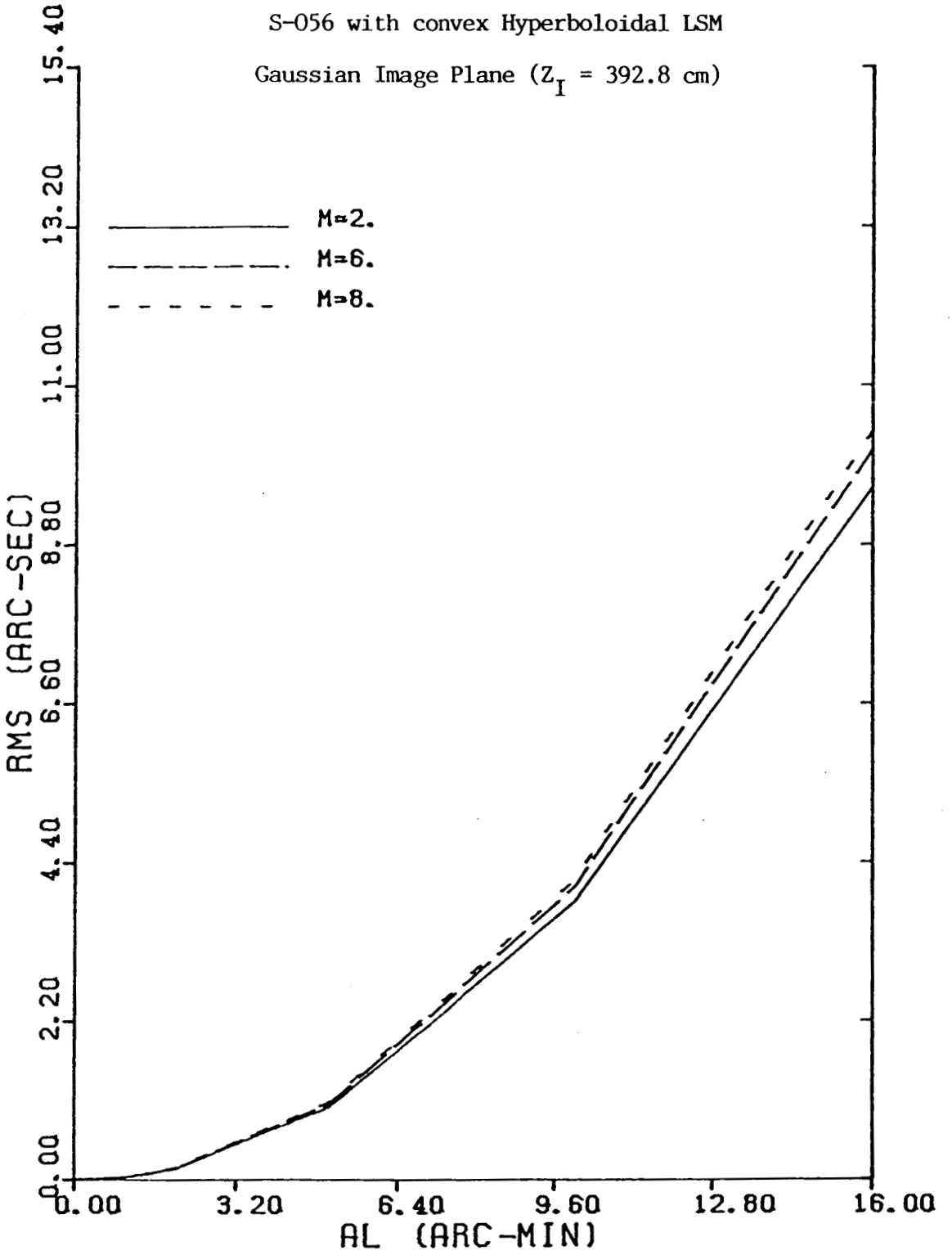

Figure 7. RMS blur circle radius as a function of field angle and magnification for a Spectral Slicing X-Ray Telescope with a Wolter I primary and convex hyperboloidal LSM.

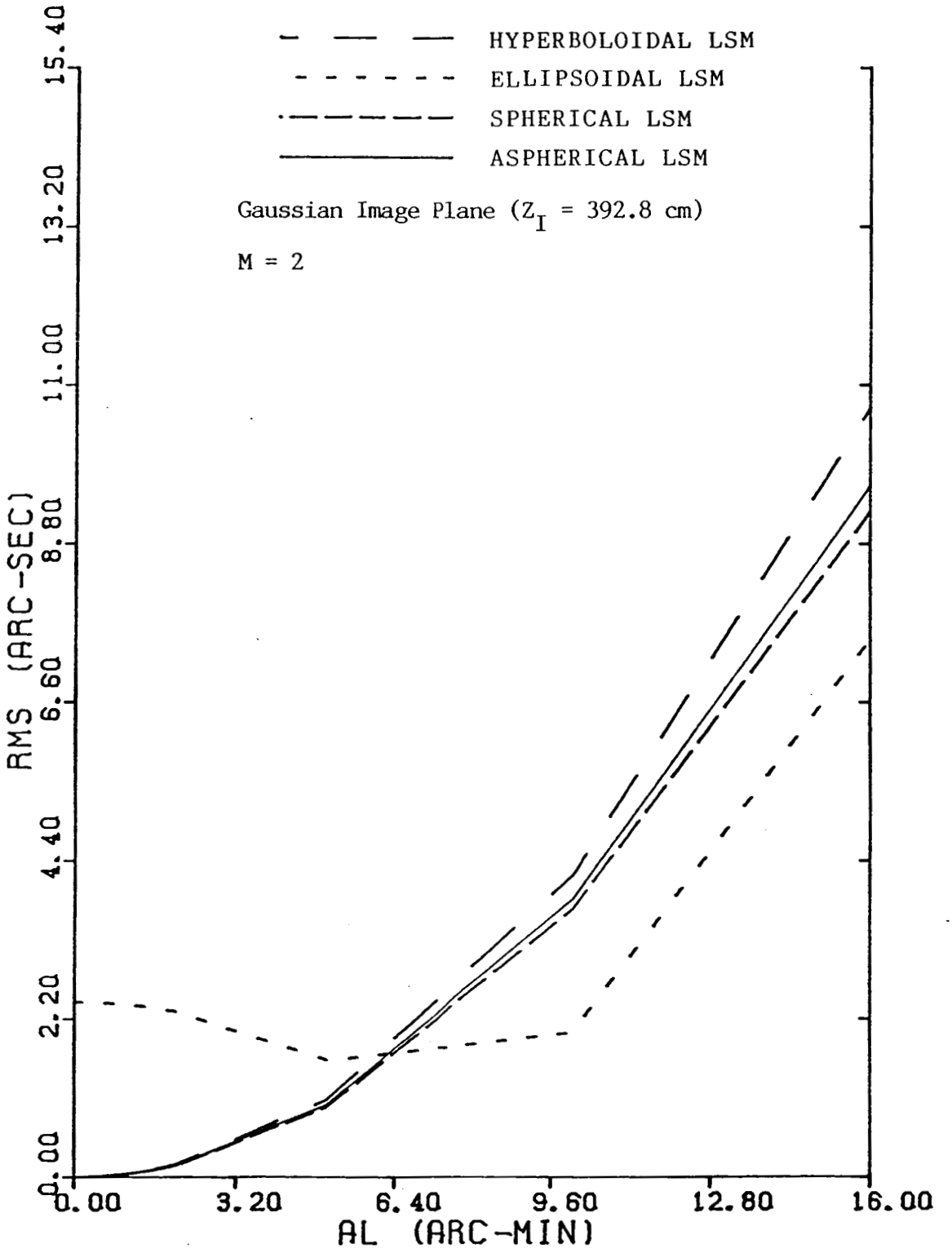

Figure 8. RMS blur circle radius as a function of field angle for magnification 2X LSM optics of different contours with S-056 primary. (Gaussian focal plane).

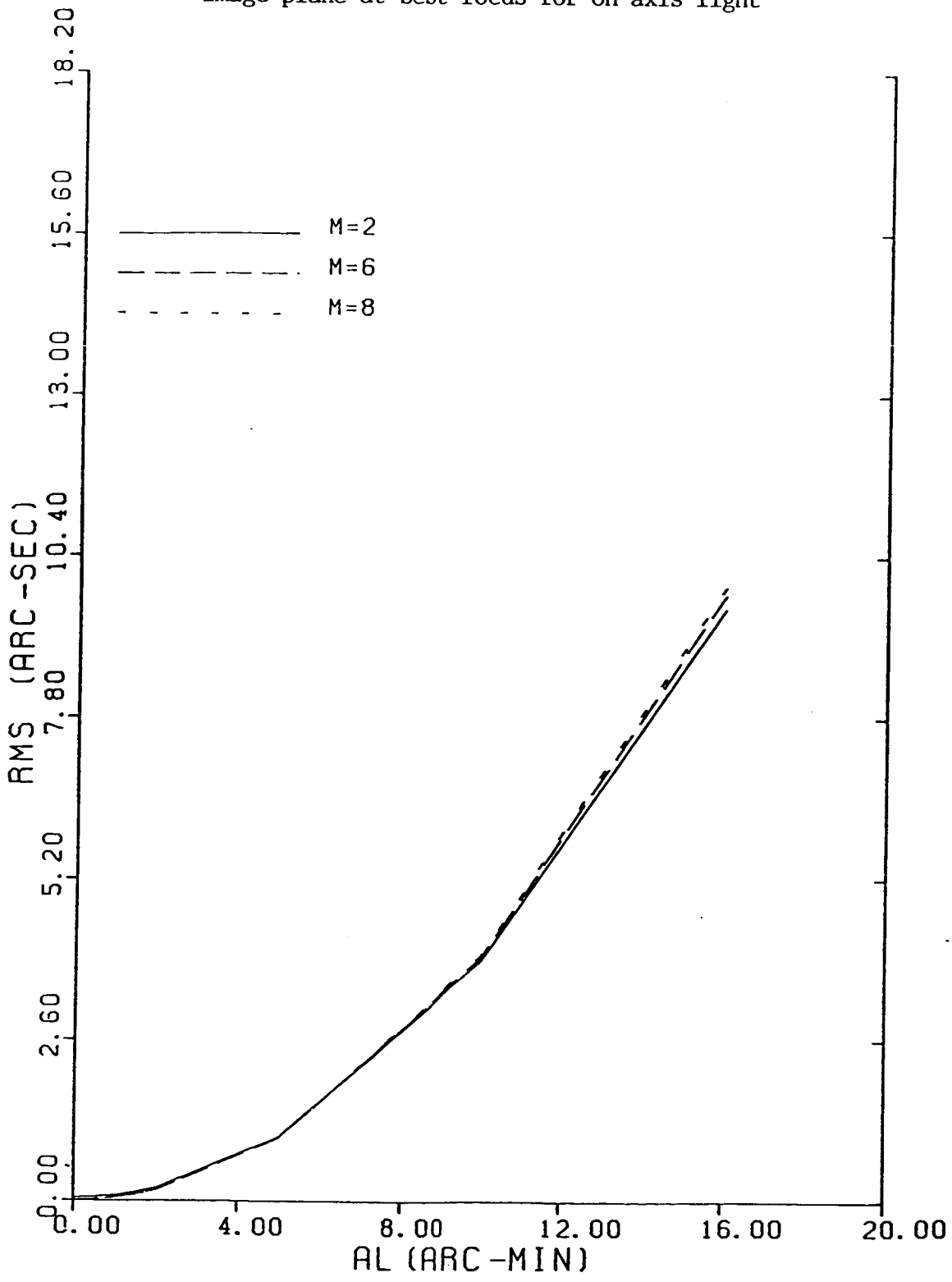

Figure 9. RMS blur circle radius versus field angle for S-056 primary and convex spherical LSM secondary for image at best focus for on-axis light.

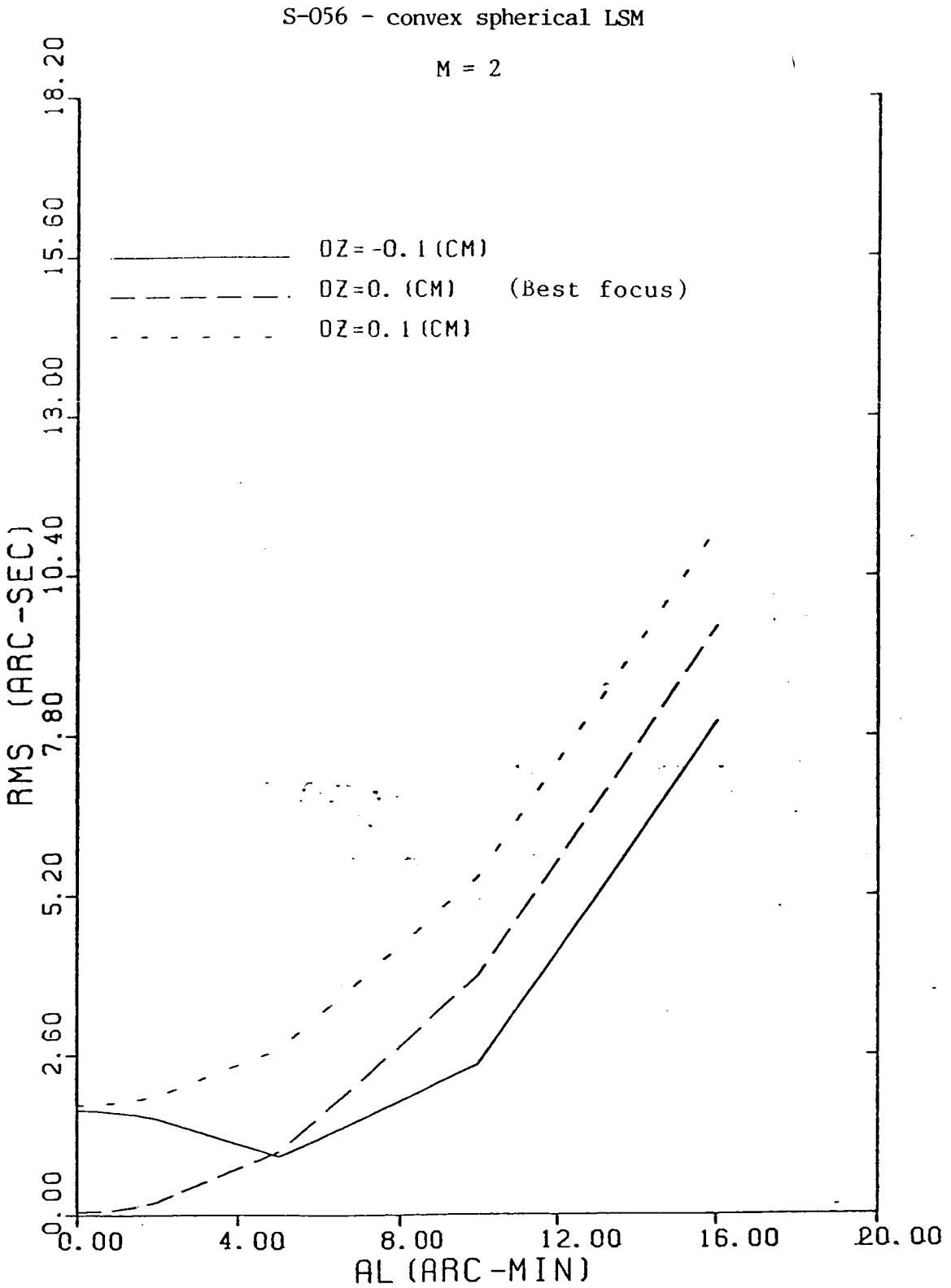

Figure 10. RMS blur circle radius versus field angle for S-056 and convex spherical LSM secondary when image plane is defocused by amount DZ from point of best focus.

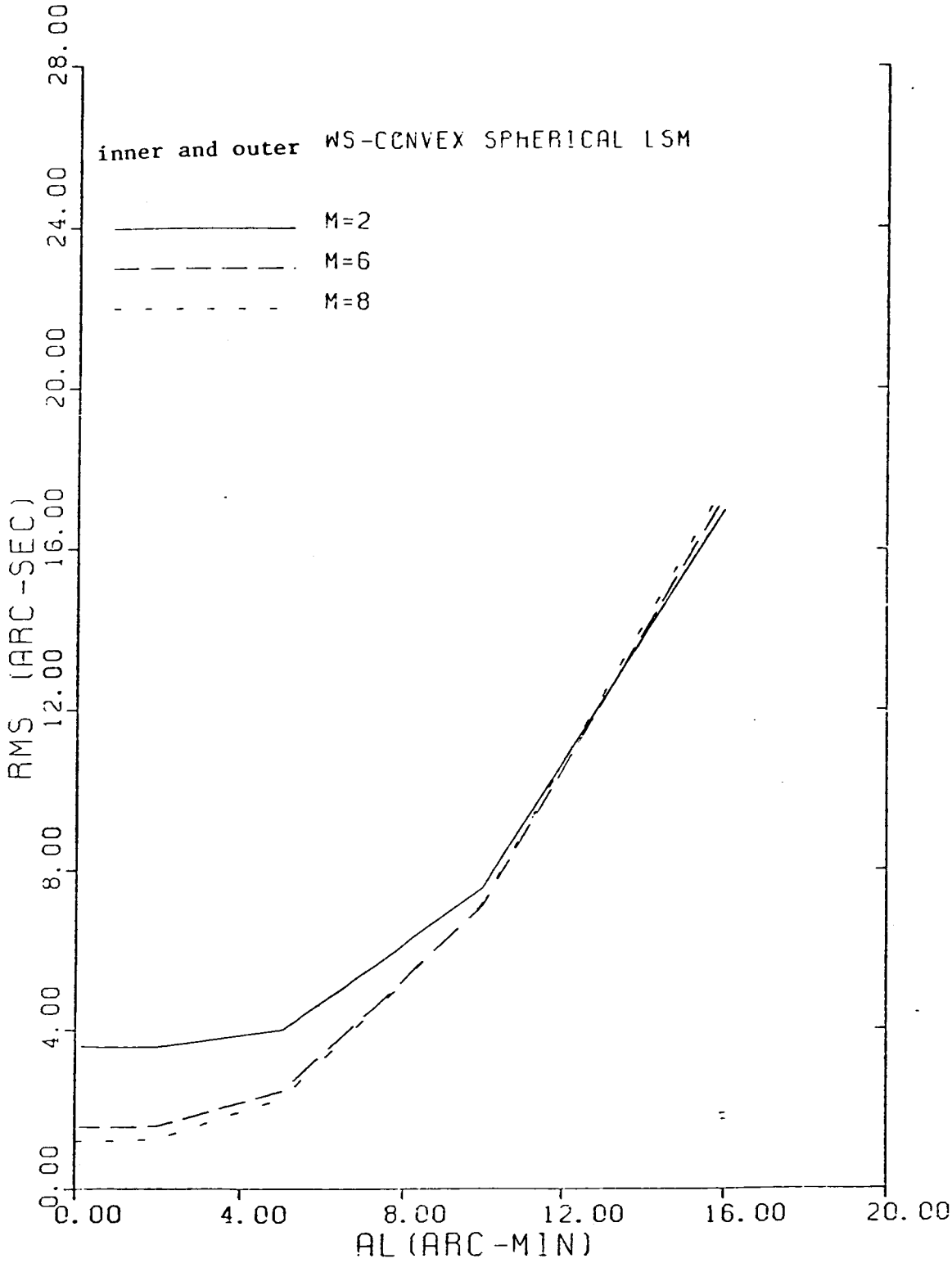

Figure 11. RMS blur circle radius versus field angle for Stanford/MSFC nested WS primary with convex spherical LSM secondary for image plane at Gaussian focal point.

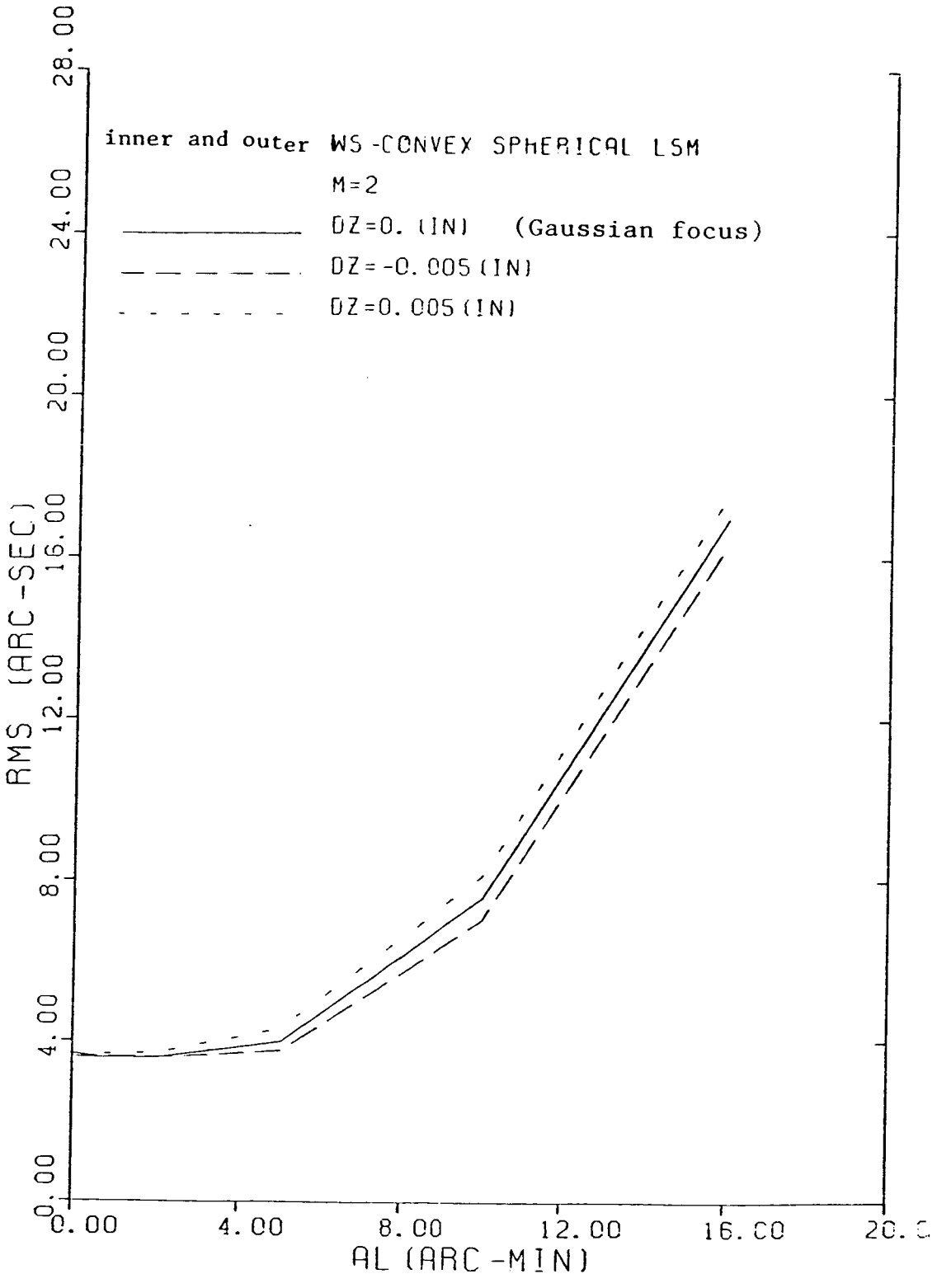

Figure 12. RMS blur circle radius versus field angle for Stanford/MSFC nested WS primary with convex spherical LSM secondary when the image plane is displaced from the Gaussian focal point.

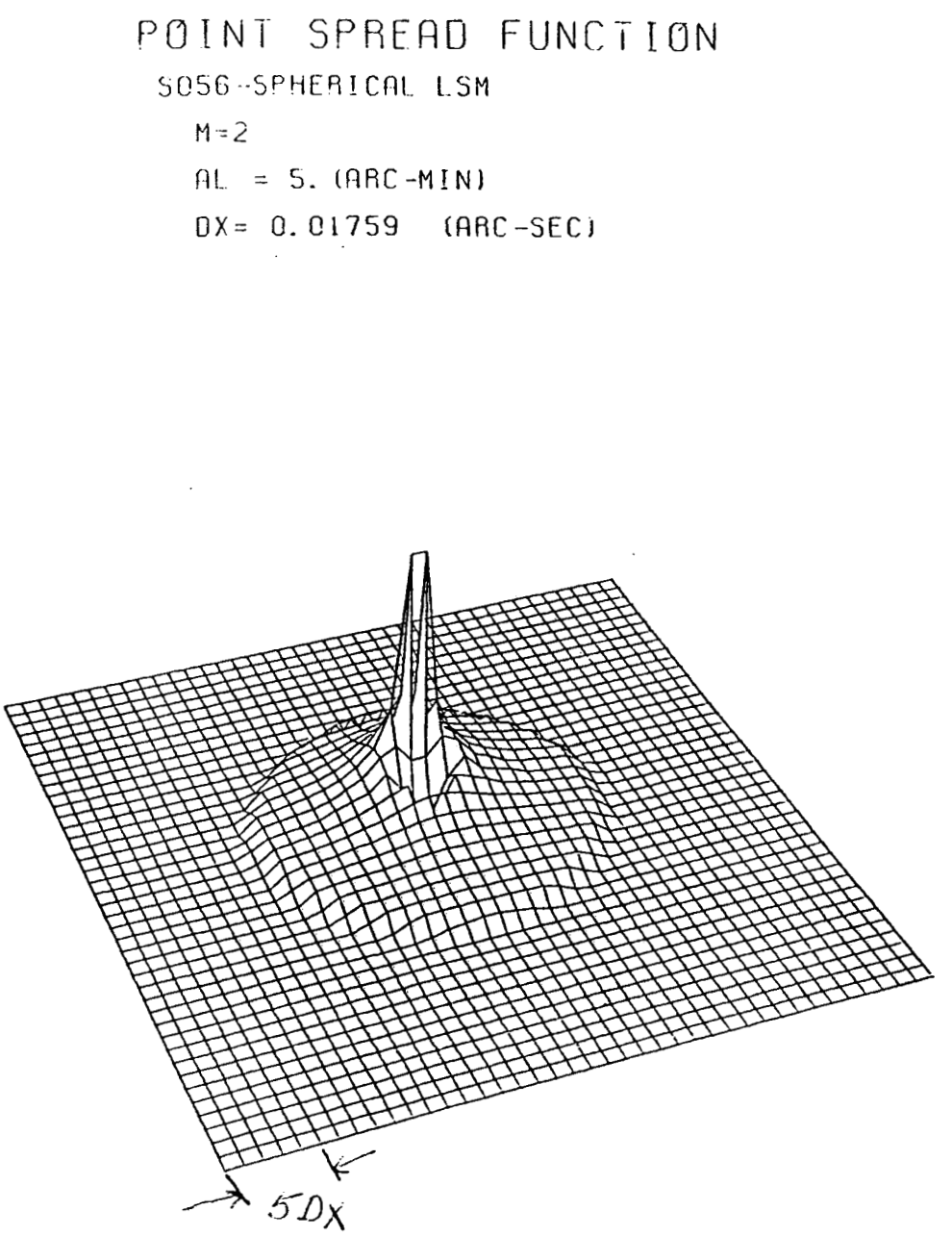

Figure 13. Point spread function for S-056 primary and spherical LSM secondary on the best focus plane with M=2 and field angle AL=5 arc-mins.

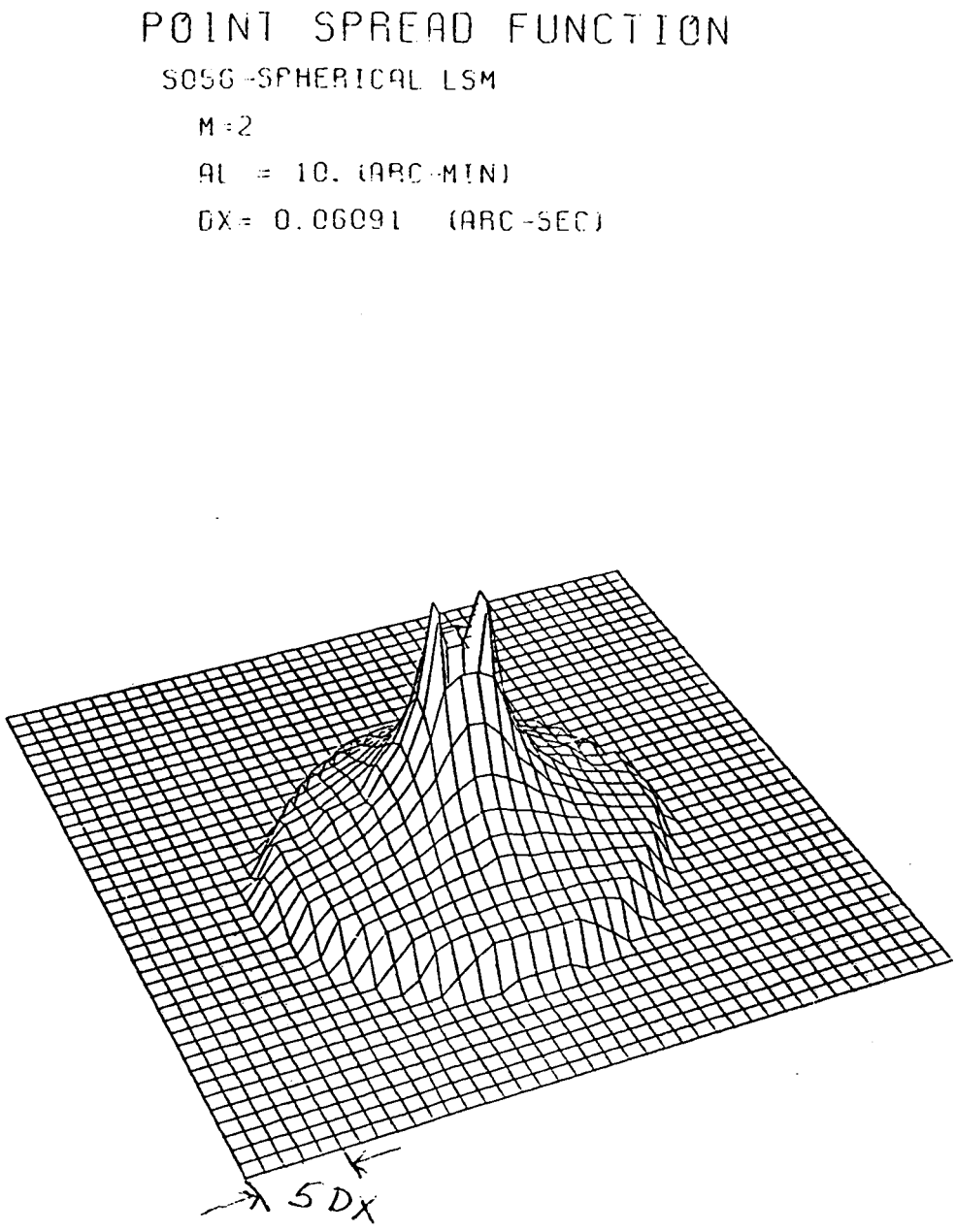

Figure 14. Point spread function for S-056 primary and spherical LSM secondary on the best focus plane with M=2 and field angle AL=10 arc-mins.

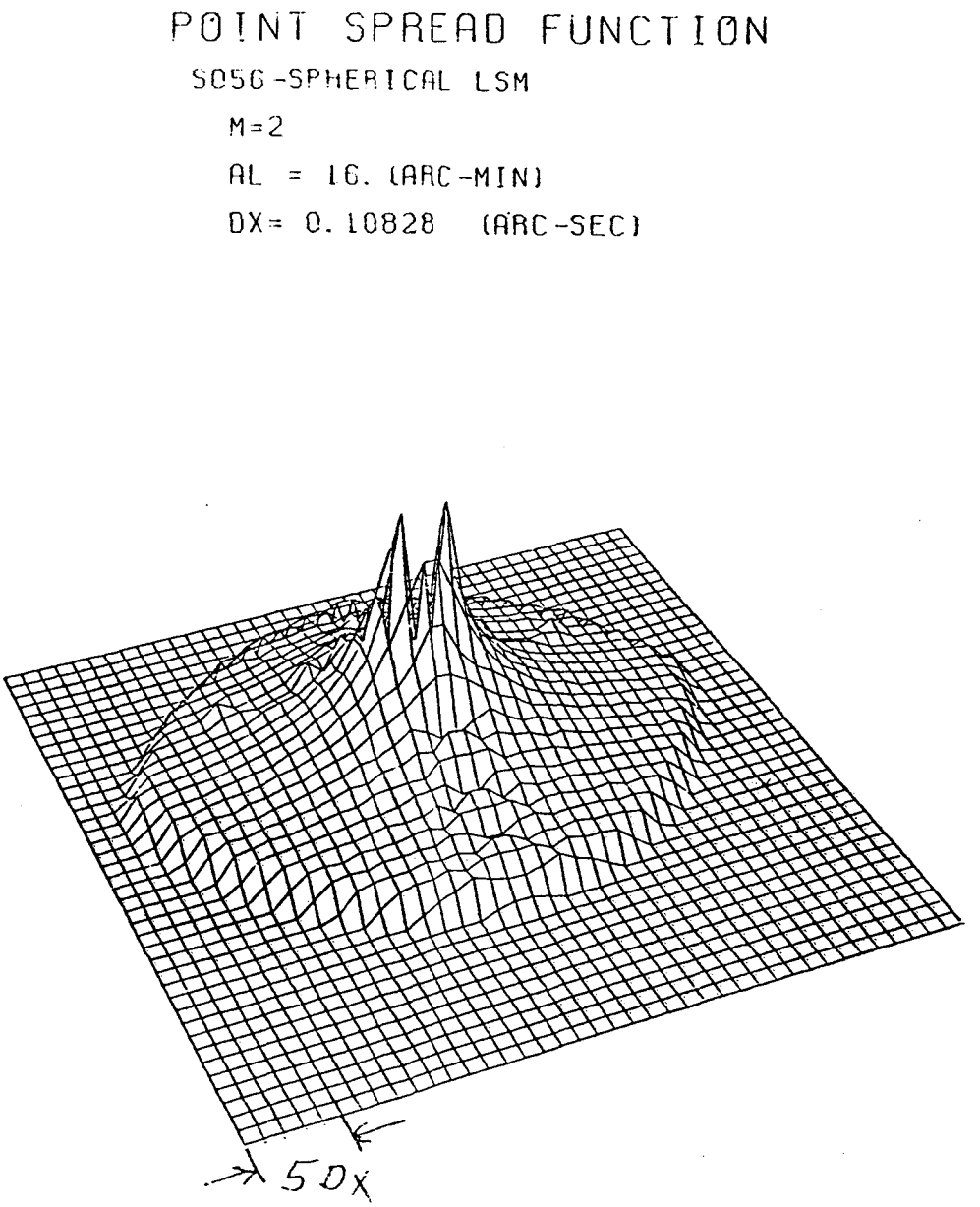

Figure 15. Point spread function for S-056 primary and spherical LSM secondary on the best focus plane with M=2 and field angle AL=16 arc-mins.

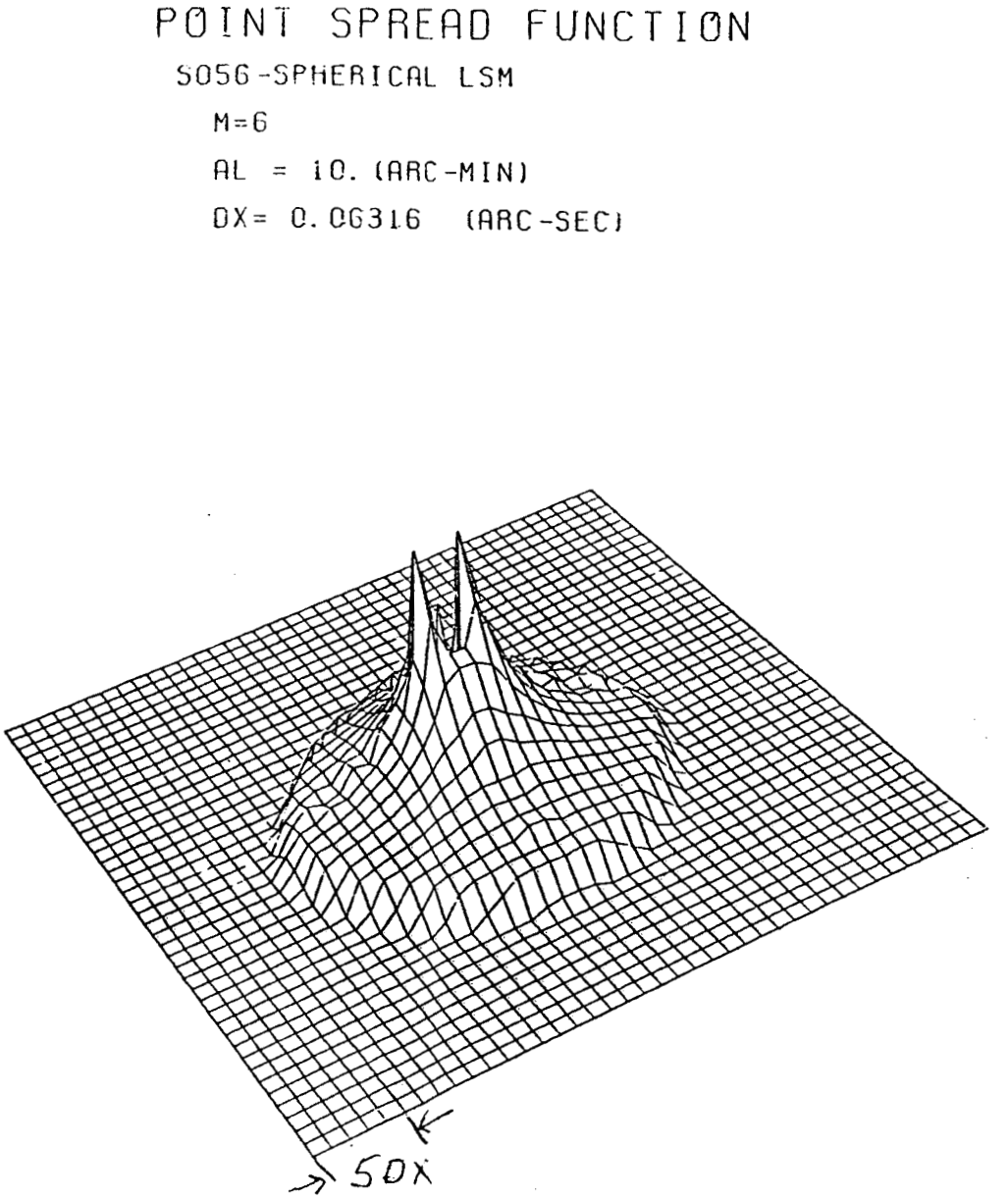

Figure 16. Point spread function for S-056 primary and spherical LSM secondary on the best focus plane with M=6 and field angle AL=10 arc-mins.

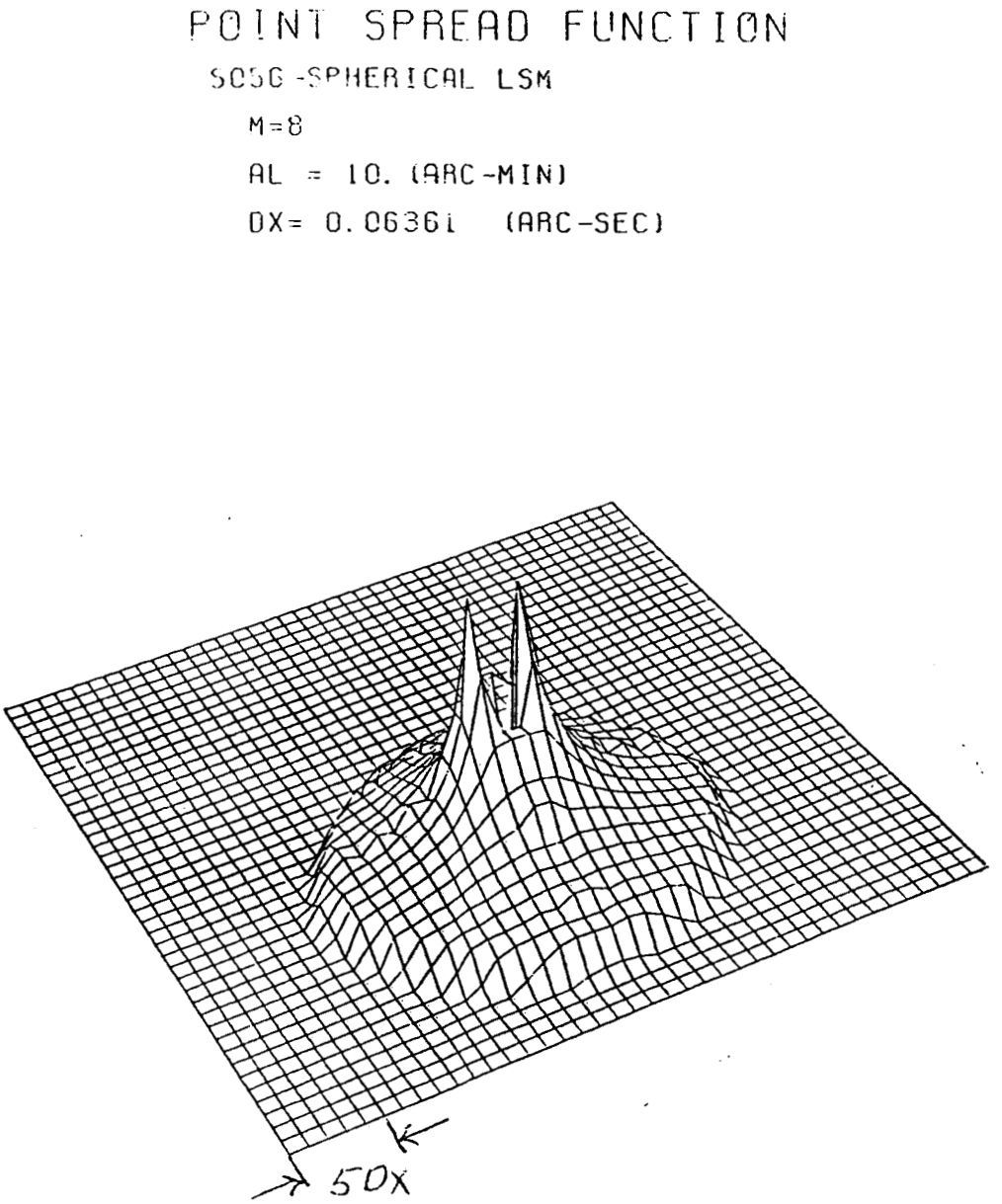

Figure 17. Point spread function for S-056 primary and spherical LSM secondary on the best focus plane with M=8 and field angle AL=10 arc-mins.

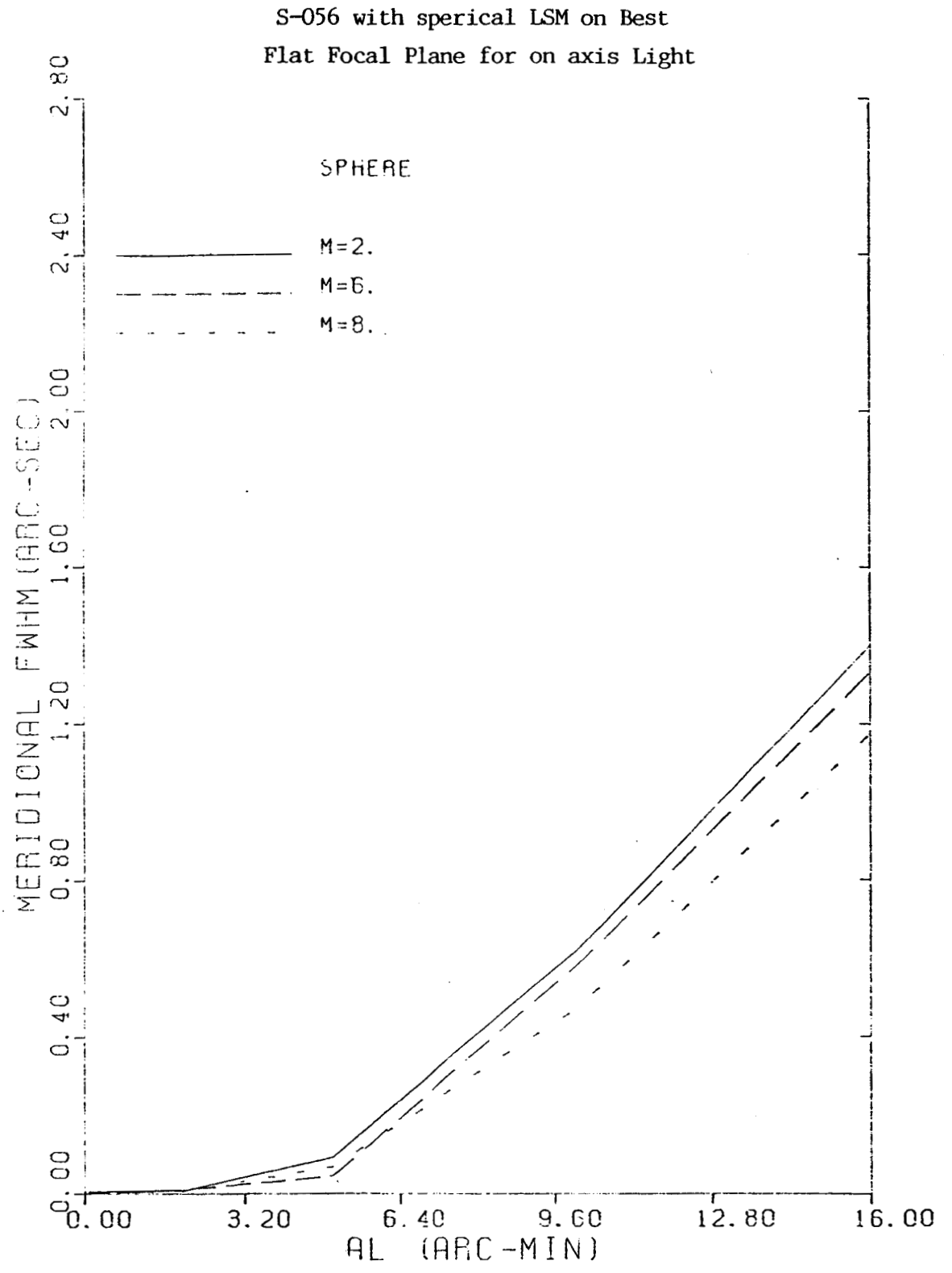

Figure 18. Full width half maximum of the meridional section of the point spread function for S-056 primary and convex spherical LSM secondary on best flat focal plane for on axis light.

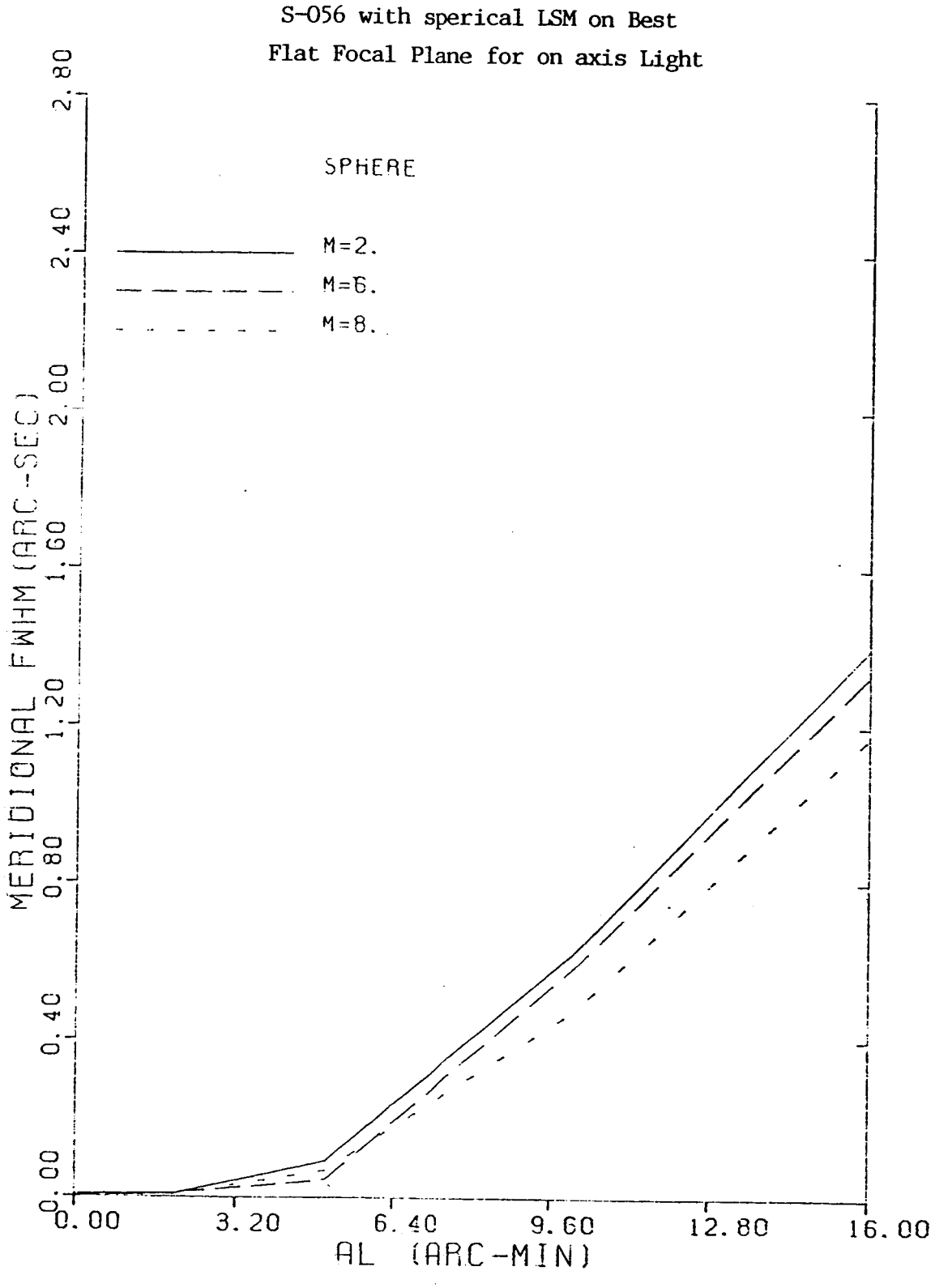

Figure 18. Full width half maximum of the meridional section of the point spread function for S-056 primary and convex spherical LSM secondary on best flat focal plane for on axis light.

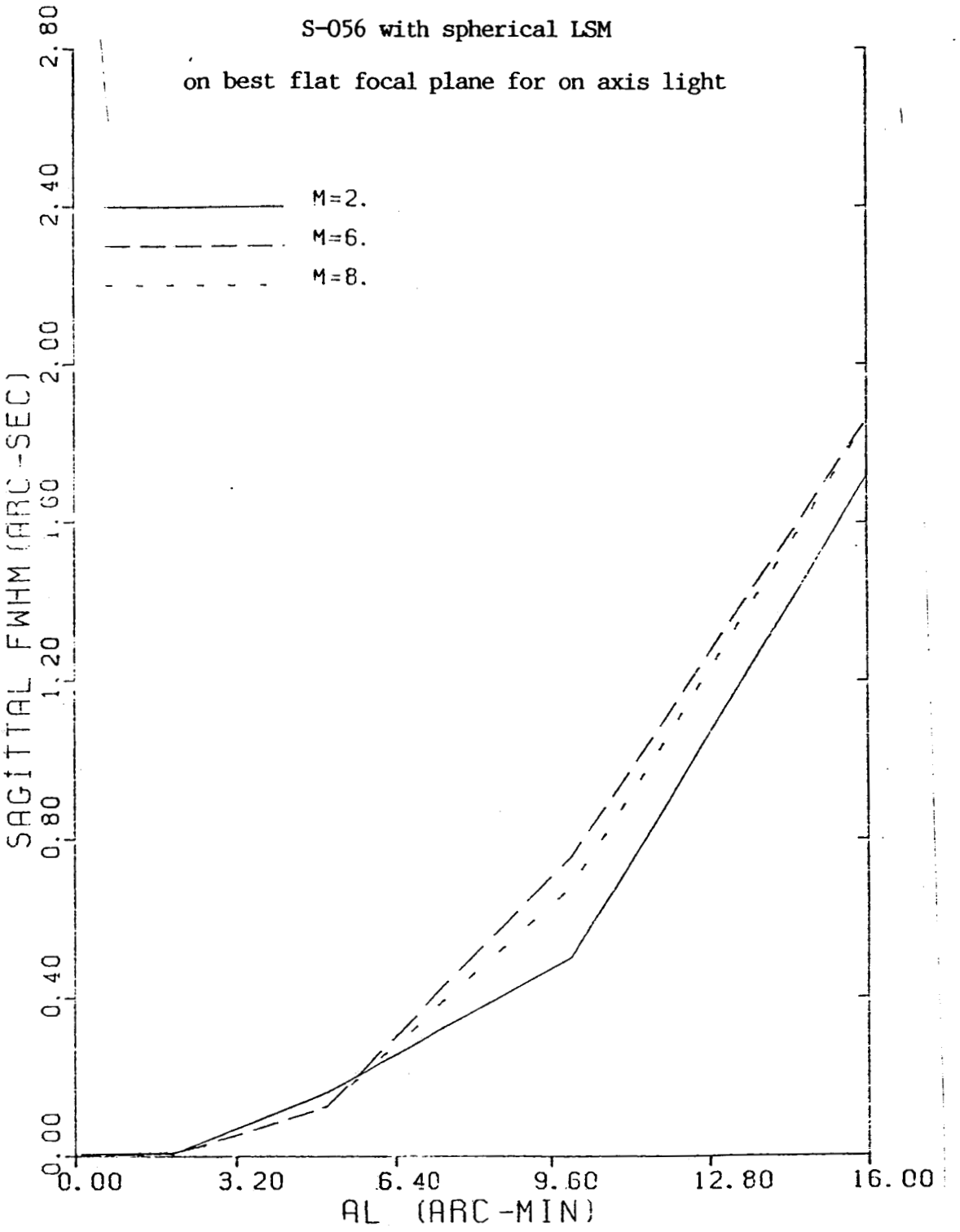

Figure 19. Full width half maximum of the sagittal section of the point spread function for S-056 primary and convex spherical LSM secondary on best flat focal plane for on axis light versus the field angle.

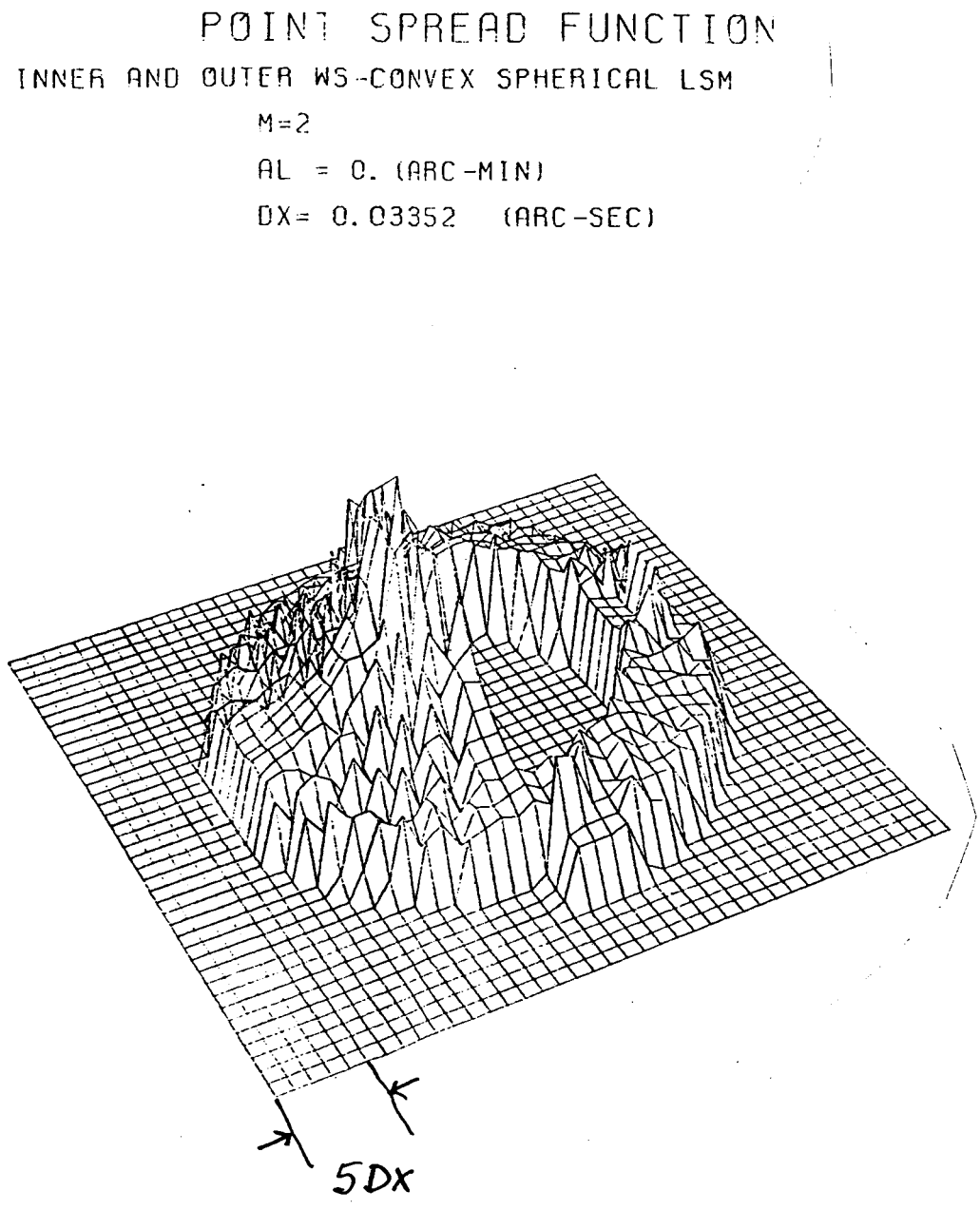

Figure 20. Point spread function of the Stanford/MSFC nested WS primary and convex spherical LSM secondary on best focal plane with M=2 and field angle AL=0. Rays were traced through only half of the entrance pupil.

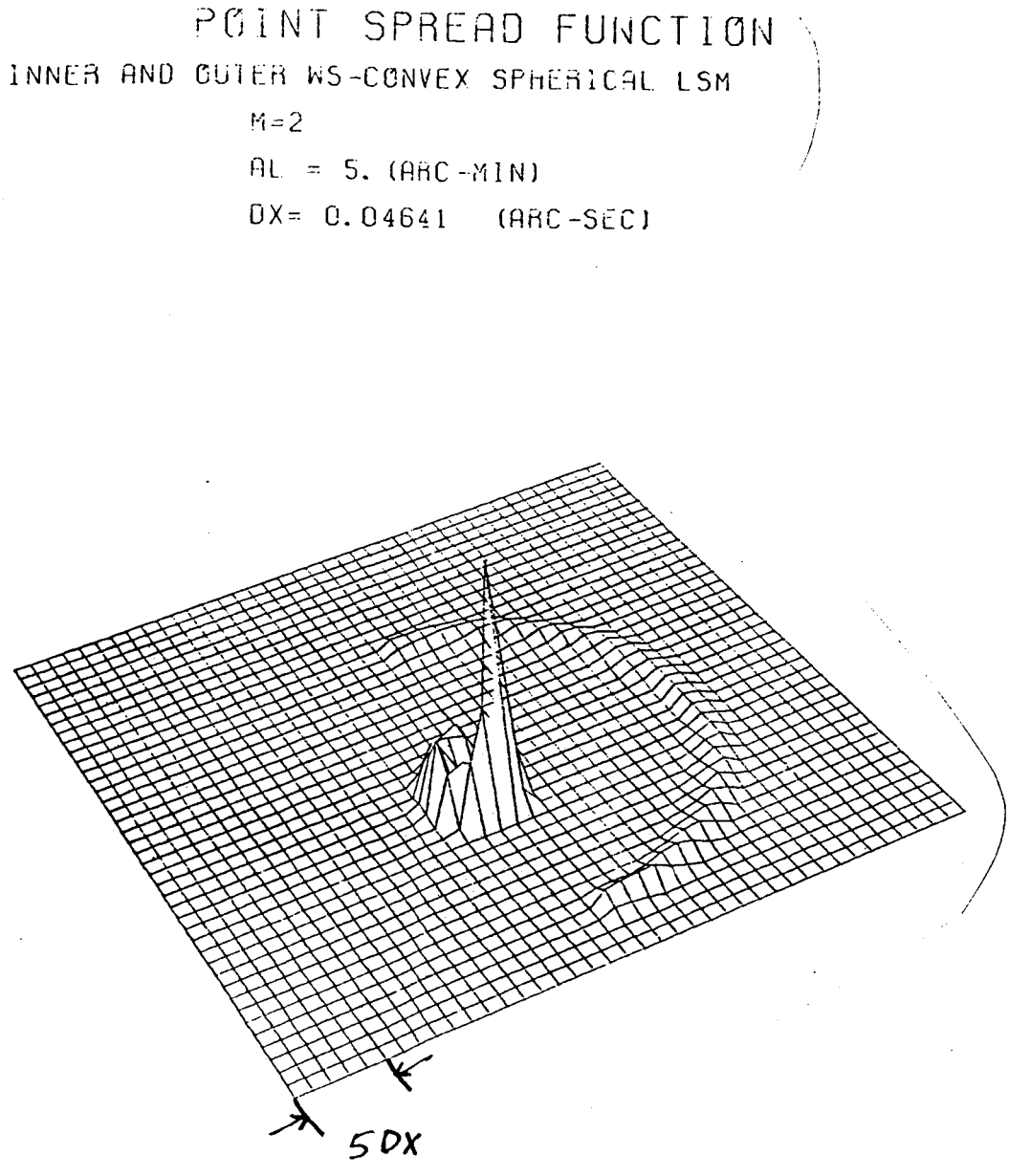

Figure 21. Point spread function of the Stanford/MSFC nested WS primary and convex spherical LSM secondary on best focal plane with M=2 and field angle AL=5 arc-mins. Rays were traced through only half of the entrance pupil.

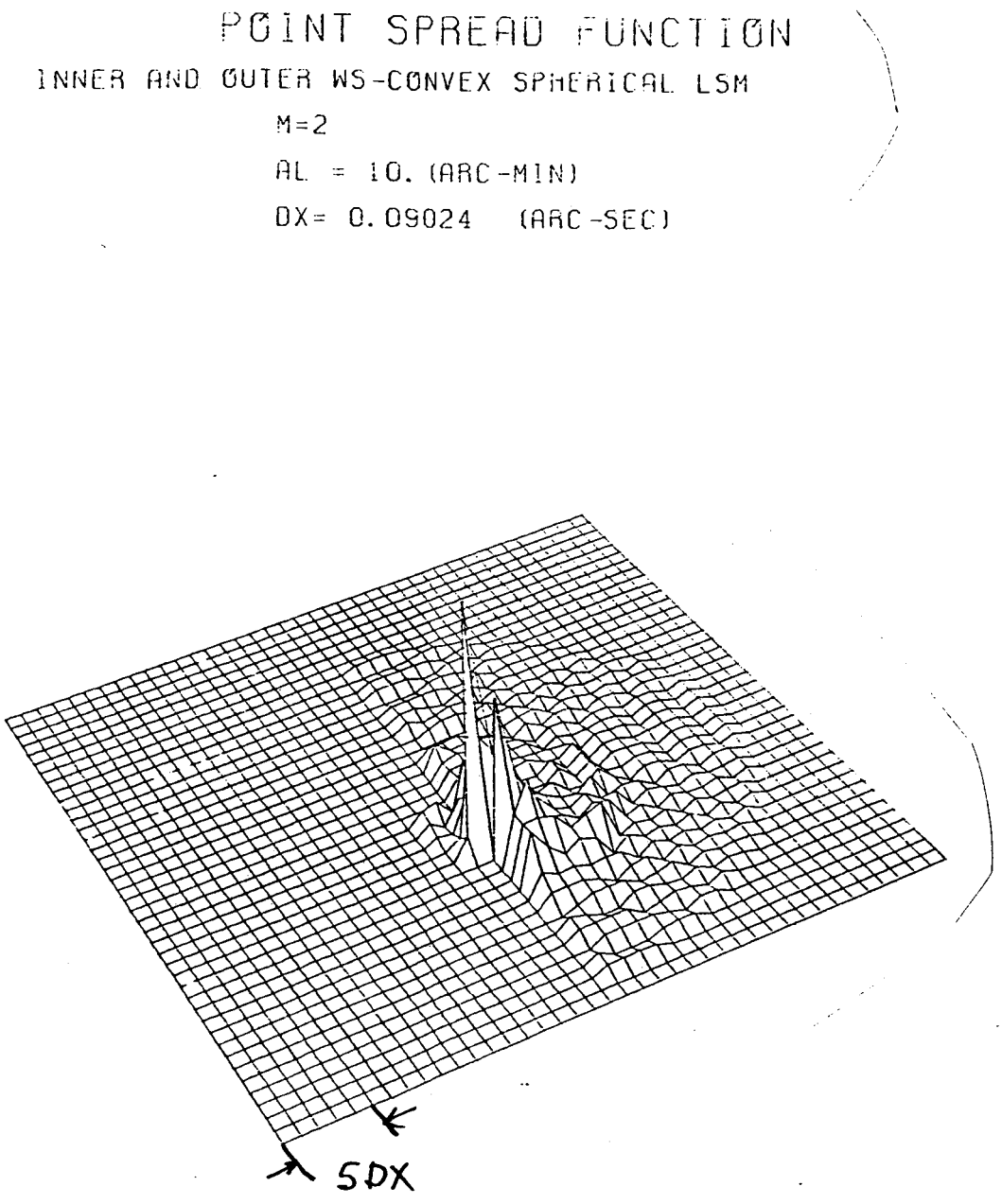

Figure 22. Point spread function of the Stanford/MSFC nested WS primary and convex spherical LSM secondary on best focal plane with M=2 and field angle AL=10 arc-mins. Rays were traced through only half of the entrance pupil.

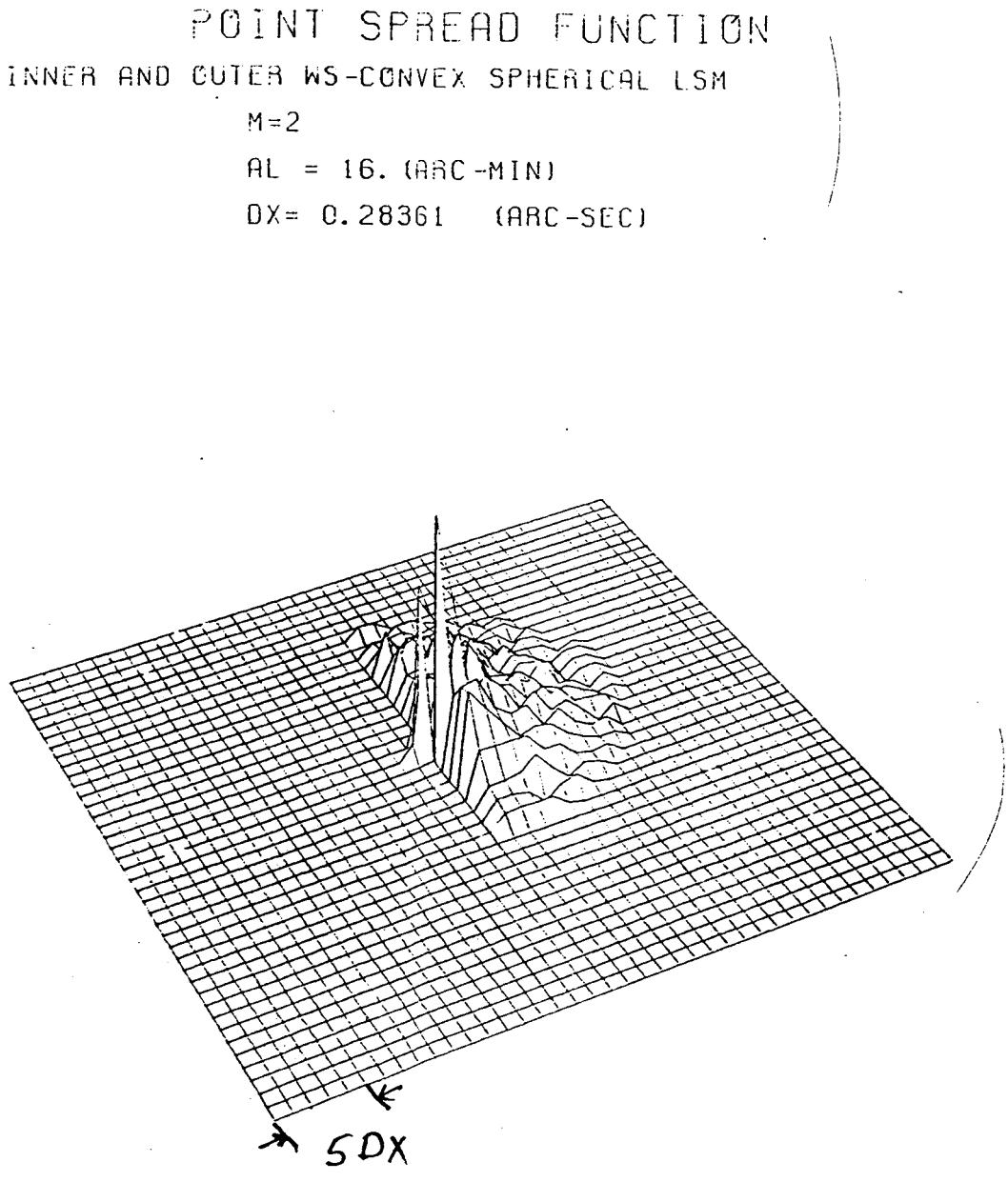

Figure 23. Point spread function of the Stanford/MSFC nested WS primary and convex spherical LSM secondary on best focal plane with M=2 and field angle AL=16 arc-mins. Rays were traced through only half of the entrance pupil.

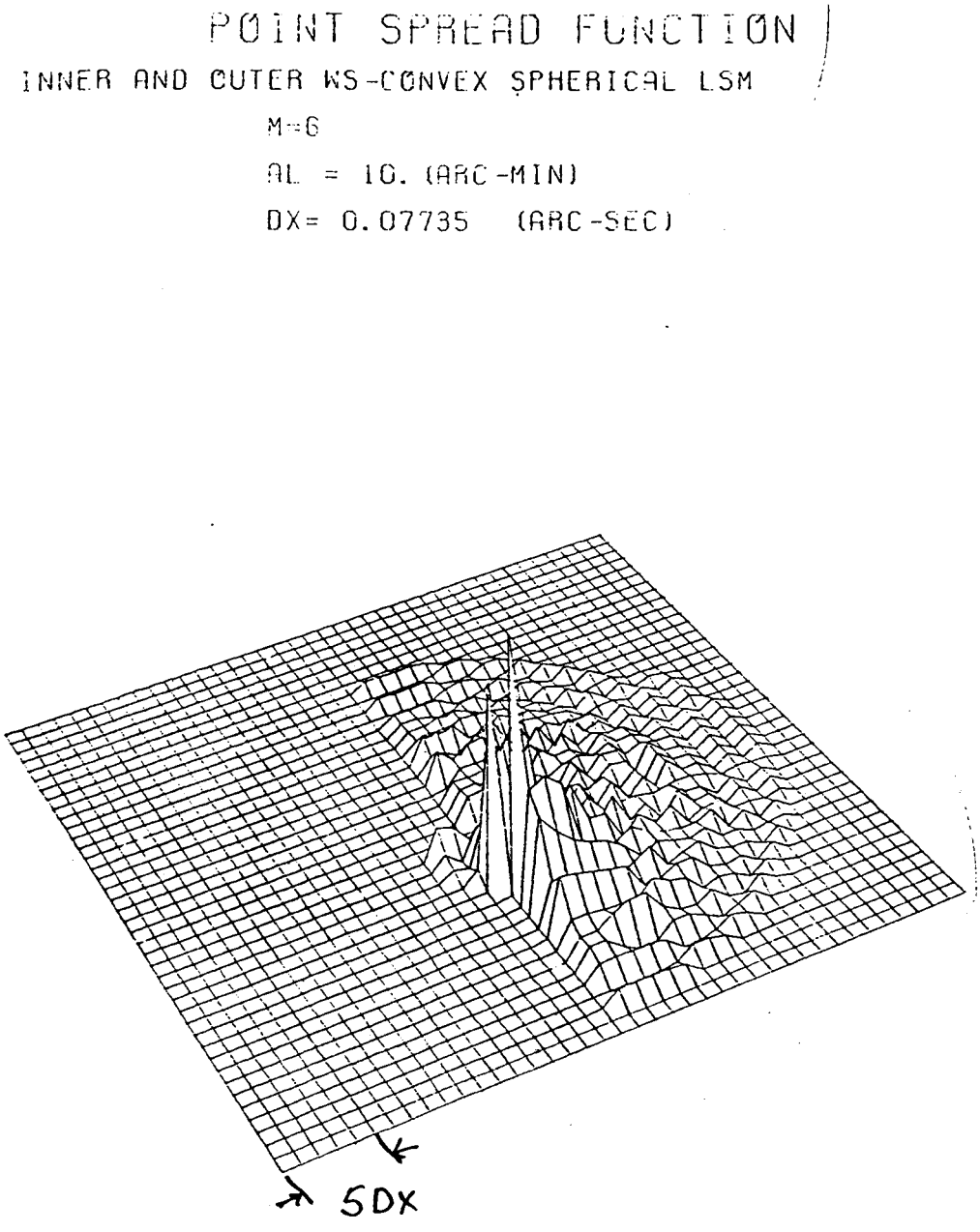

Figure 24. Point spread function of the Stanford/MSFC nested WS primary and convex spherical LSM secondary on best focal plane with M=6 and field angle AL=10 arc-mins. Rays were traced through only half of the entrance pupil.

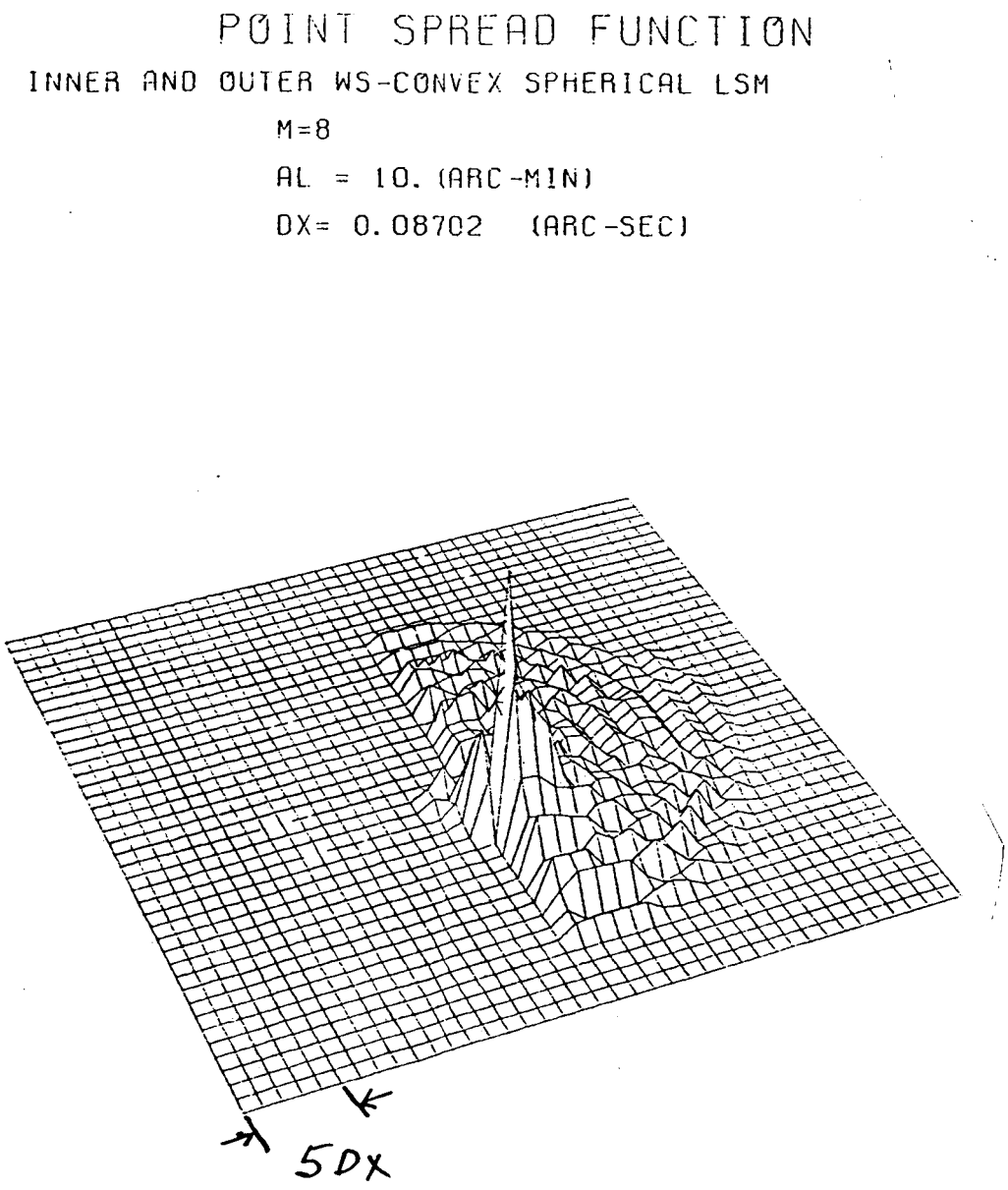

Figure 25. Point spread function of the Stanford/MSFC nested WS primary and convex spherical LSM secondary on best focal plane with M=8 and field angle AL=10 arc-mins. Rays were traced through only half of the entrance pupil.

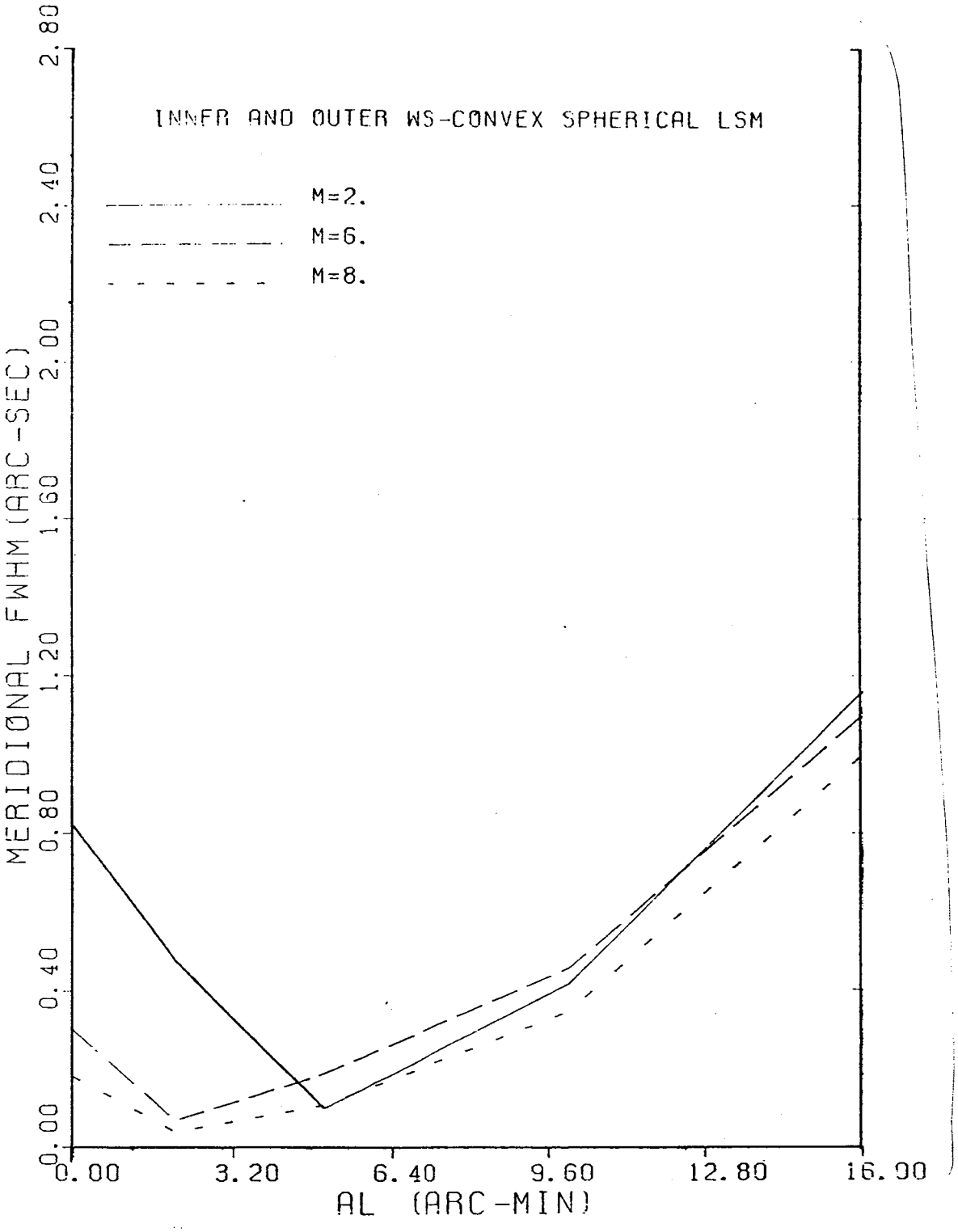

Figure 26. Full width half maximum of the meridional section of point spread function of the Stanford/MSFC nested WS primary and a convex spherical LSM secondary on best focal plane versus the field angle. Rays were traced half through half the entrance pupil.

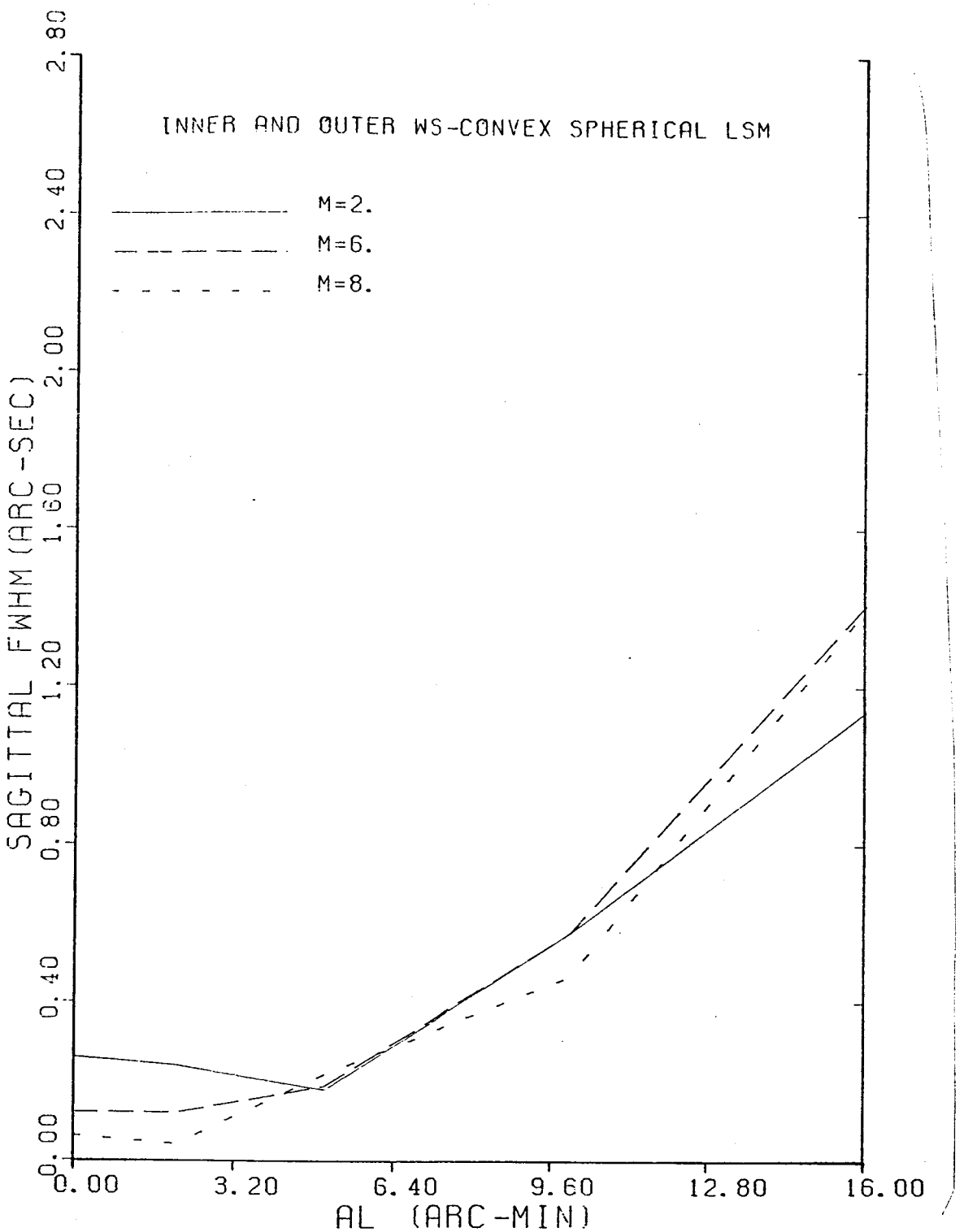

Figure 27. Full width half maximum of the sagittal section of the point spread function of the Stanford/MSFC nested WS primary and convex spherical LSM secondary on the best focal plane versus the field angle.

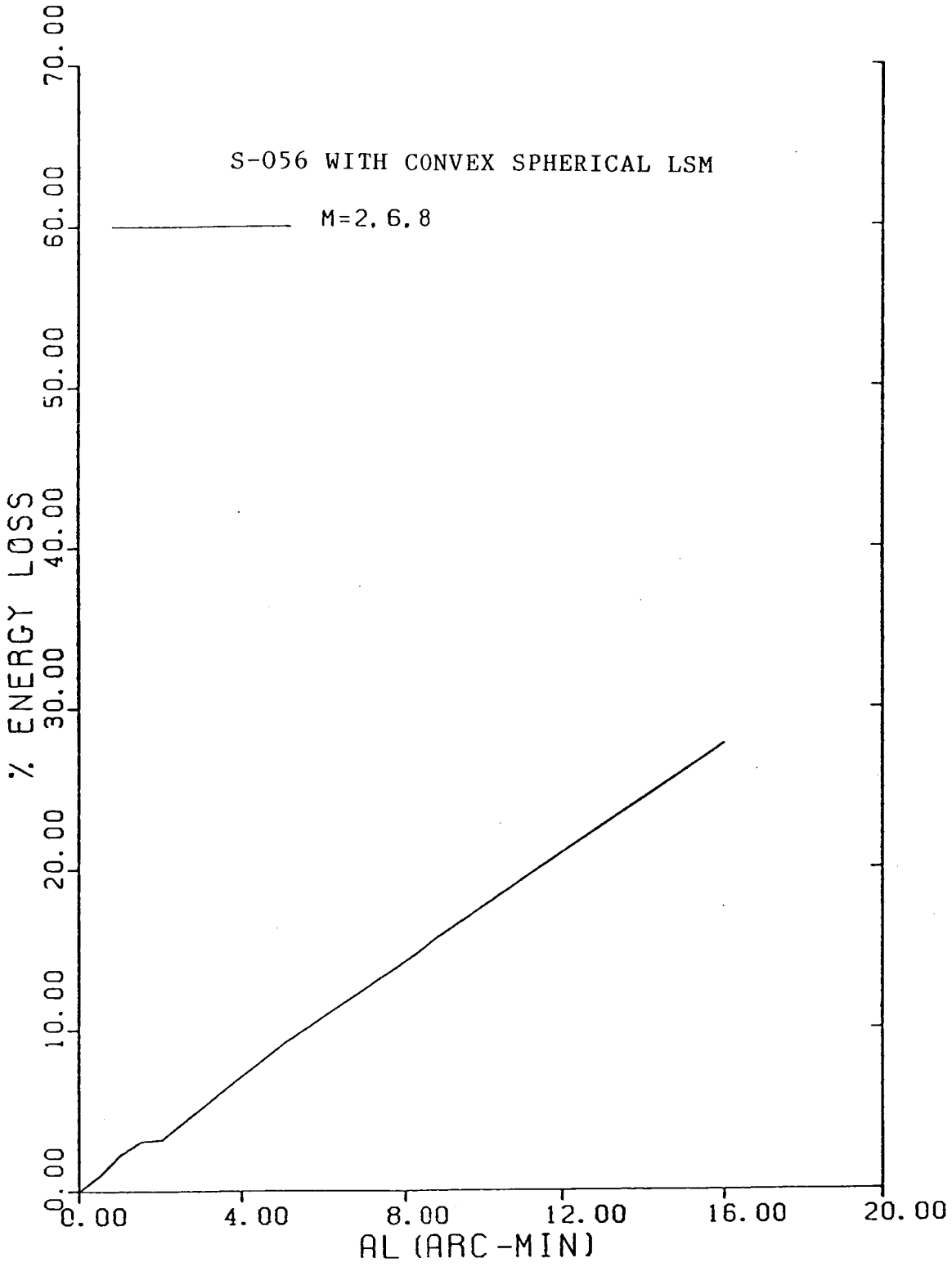

Figure 28. Percent energy loss for Spectral Slicing X-Ray Telescope with S-056 primary. (Gaussian focal plane).

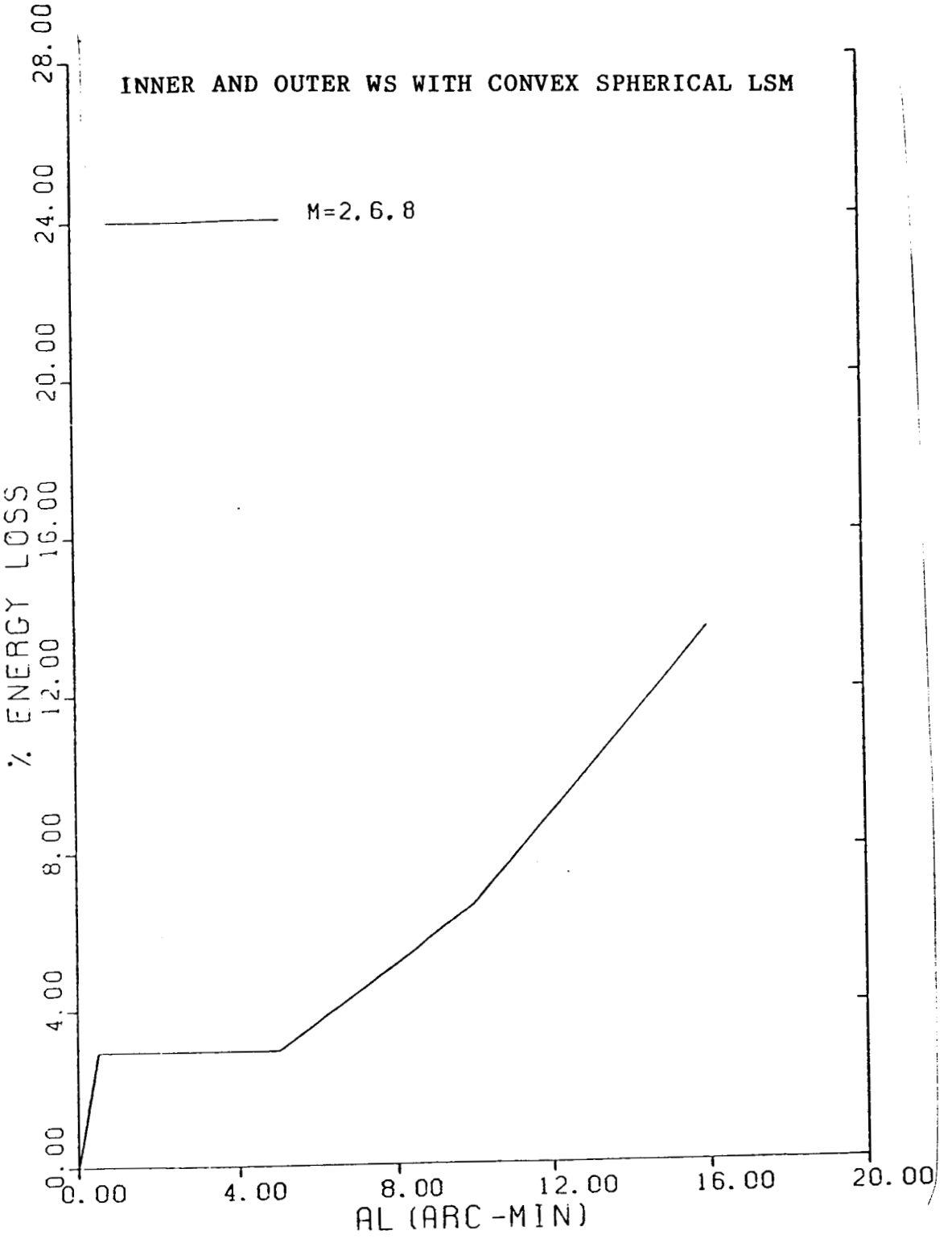

Figure 29. Percent energy loss for Spectral Slicing X-Ray Telescope with nested Wolter-Schwarzschild primary. (Gaussian focal plane).

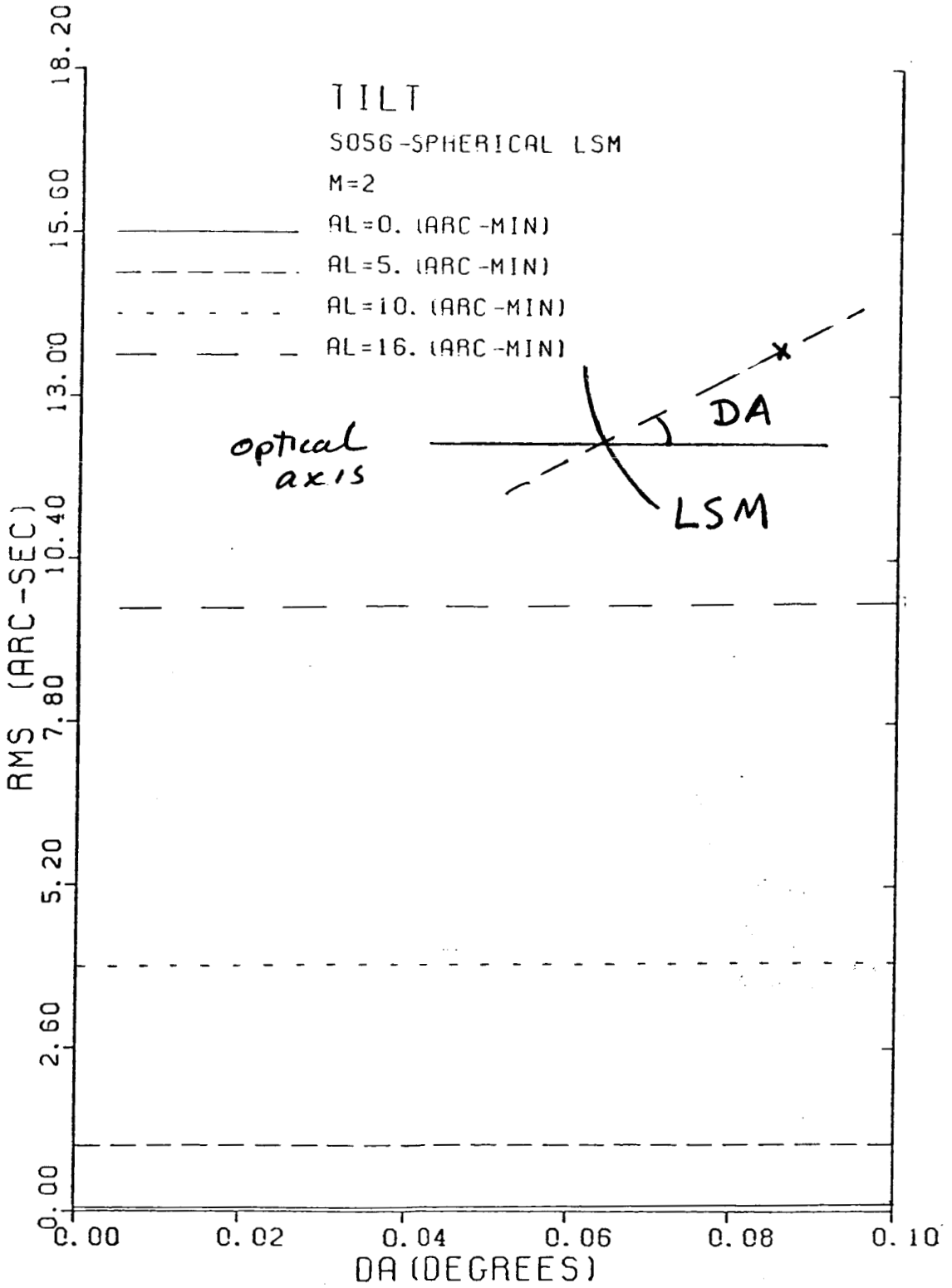

Figure 30. RMS blur circle versus the tilt angle for LSM with respect to the optical axis for S-056 primary and convex spherical secondary for M=2 and AL=0, 5, 10, 16 arc-mins.

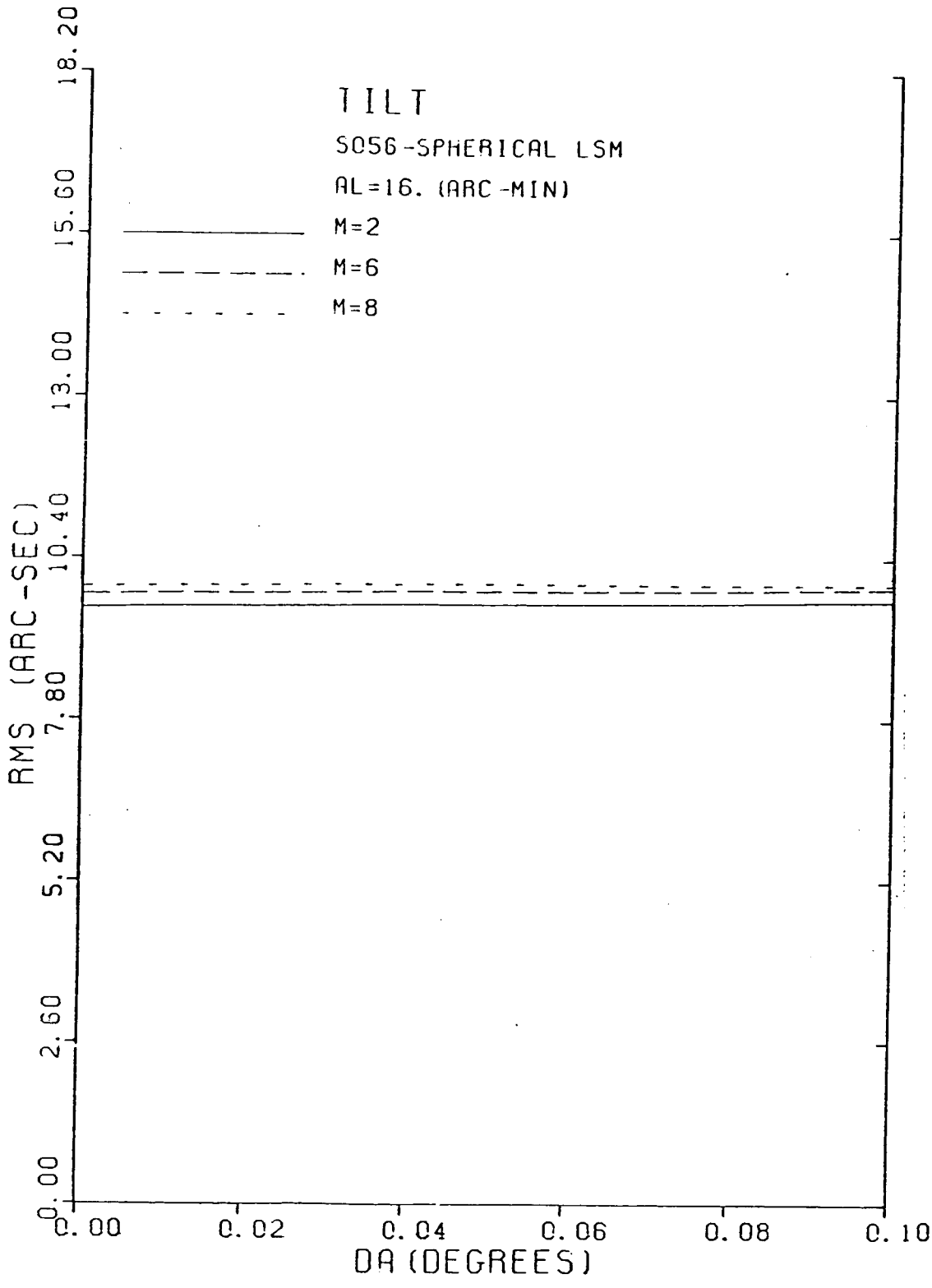

Figure 31. RMS blur circle versus the tilt angle for LSM with respect to the optical axis for S-056 primary and convex spherical secondary for M=2,6,8 and AL=16 arc-mins.

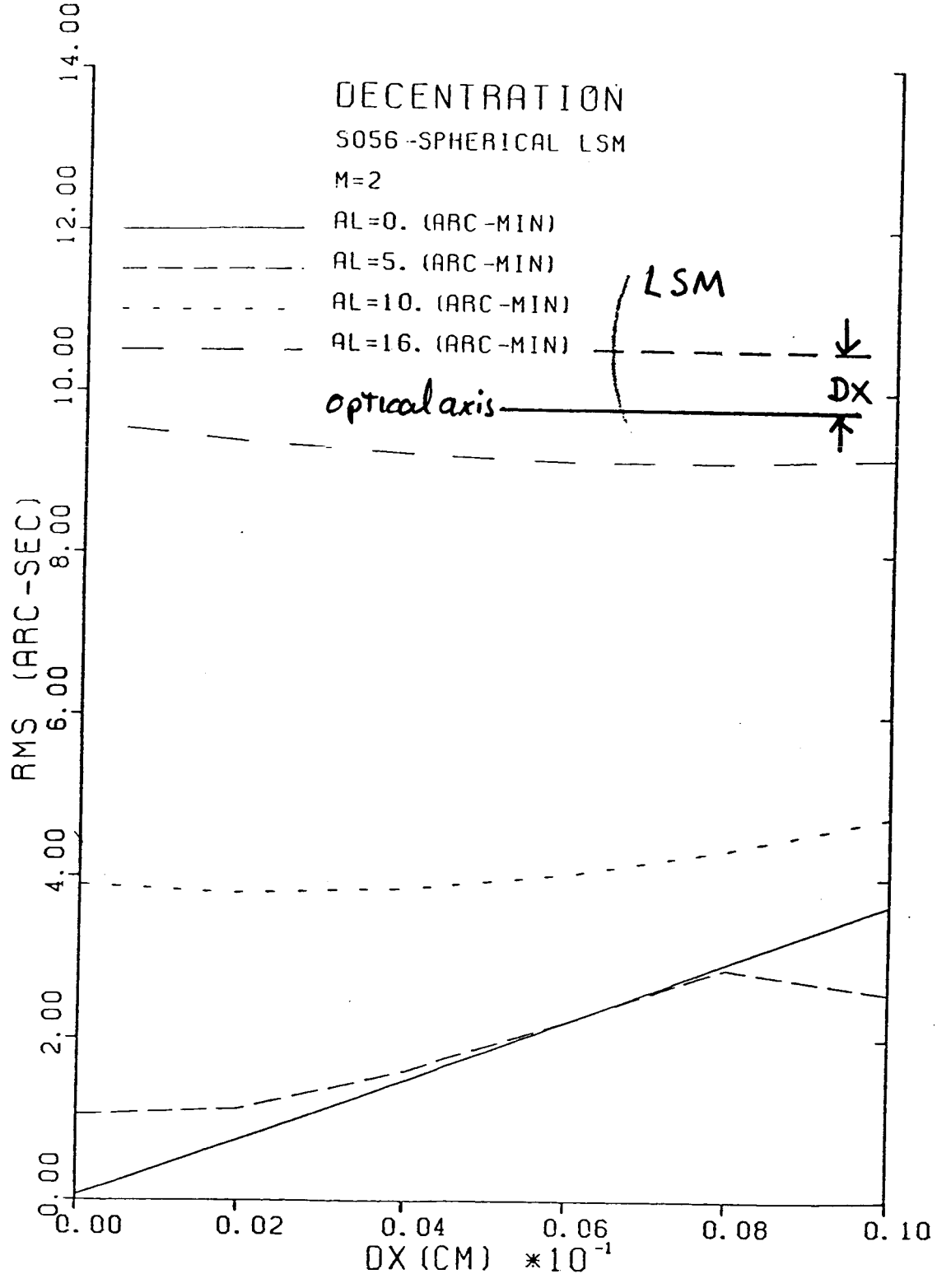

Figure 32. RMS blur circle radius versus the displacement of axis of LSM from the optical axis for S-056 primary and convex spherical LSM for M=2 and AL=0,5,10,16 arc-mins.

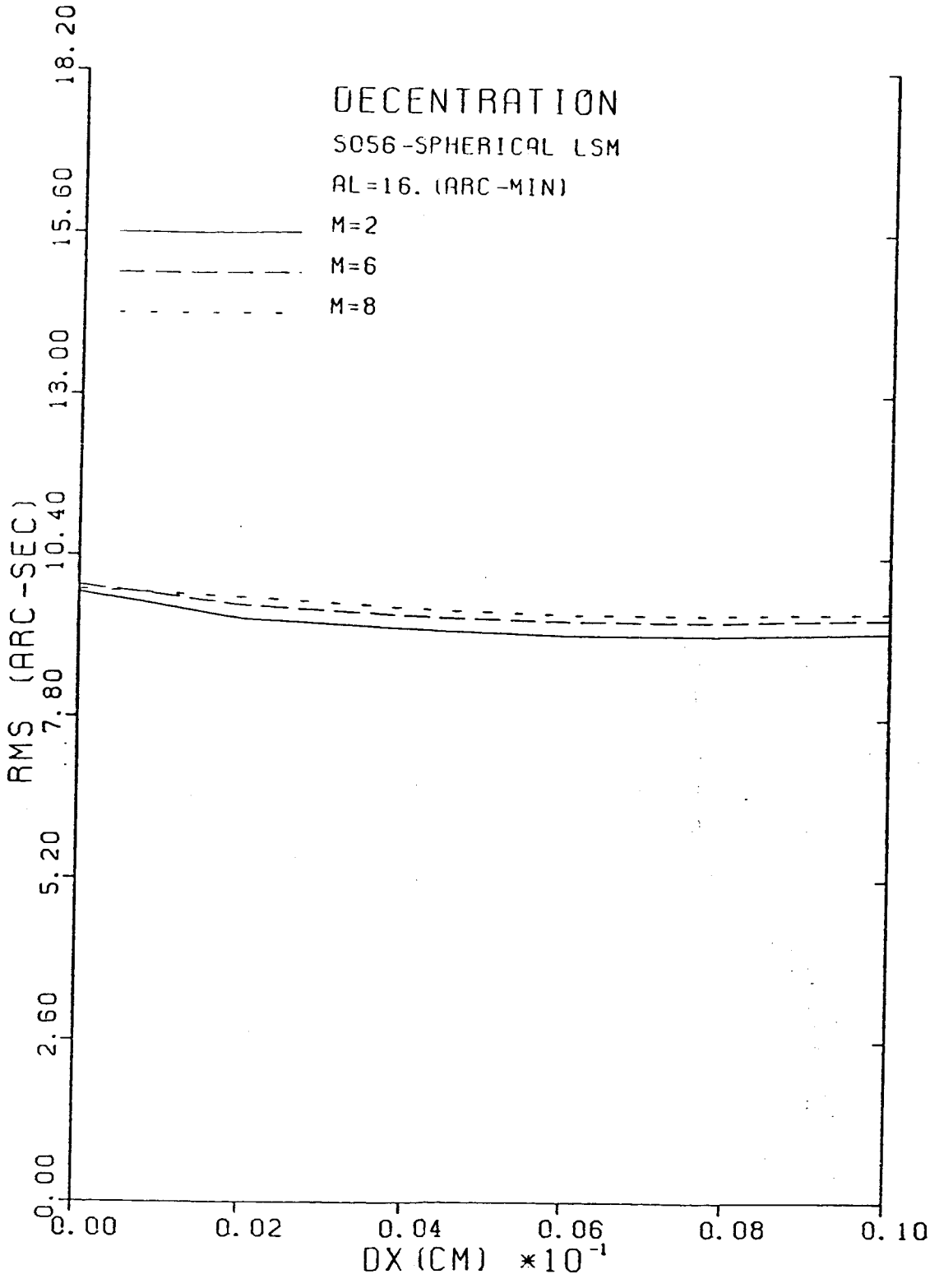

Figure 33. RMS blur circle radius versus the displacement of axis of LSM from the optical axis for S-056 primary and convex spherical LSM for M=2,6,8 and AL=16 arc-mins.

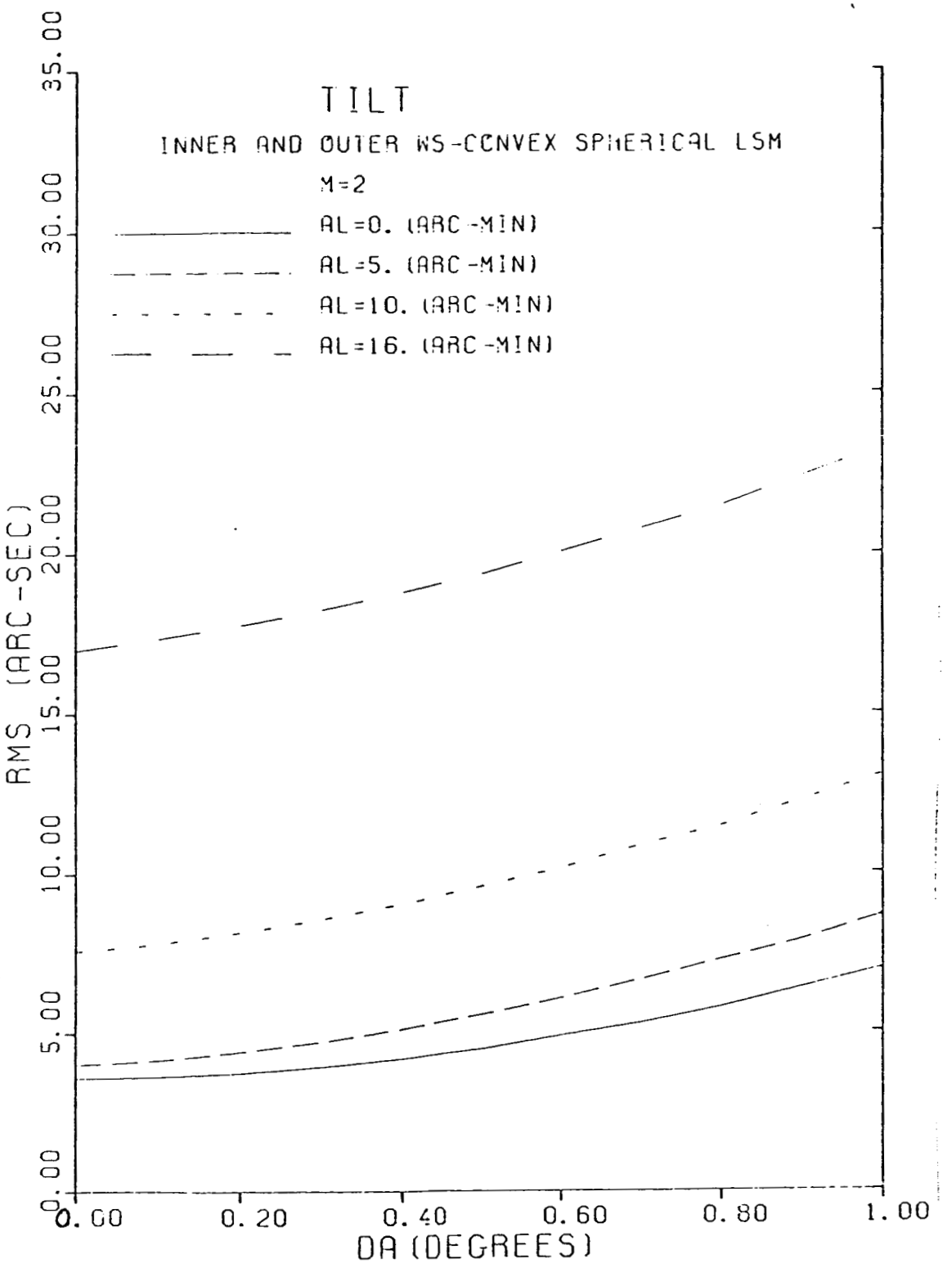

Figure 34. RMS blur circle radius versus the tilt angle for Stanford/MSFC nested WS primary and convex spherical LSM secondary for M=2 and AL=0,5,10, 16 arc-mins.

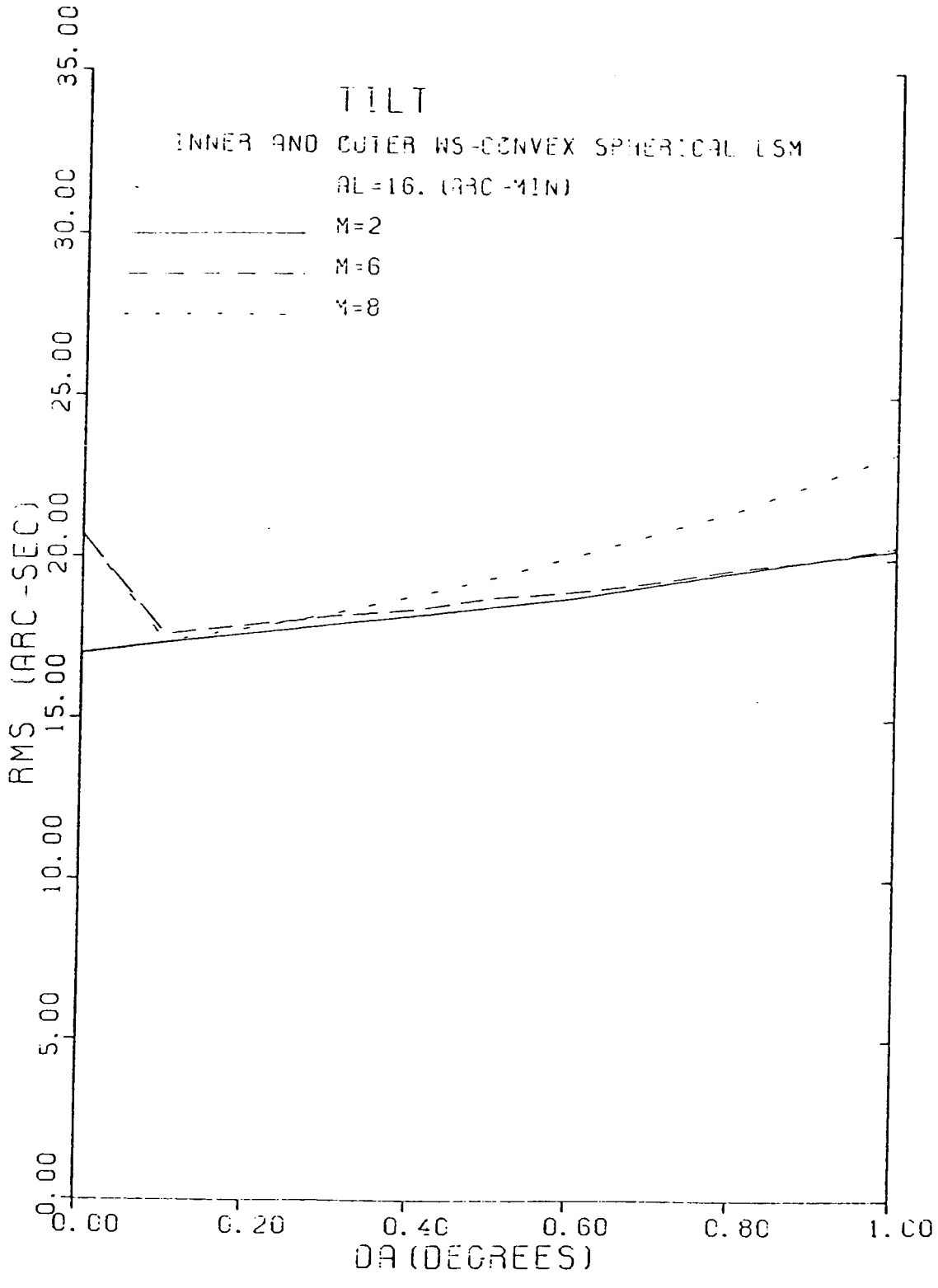

Figure 35. RMS blur circle radius versus the tilt angle for Stanford/MSFC nested WS primary and convex spherical LSM secondary for M=2,6,8 and AL=16 arc-mins.

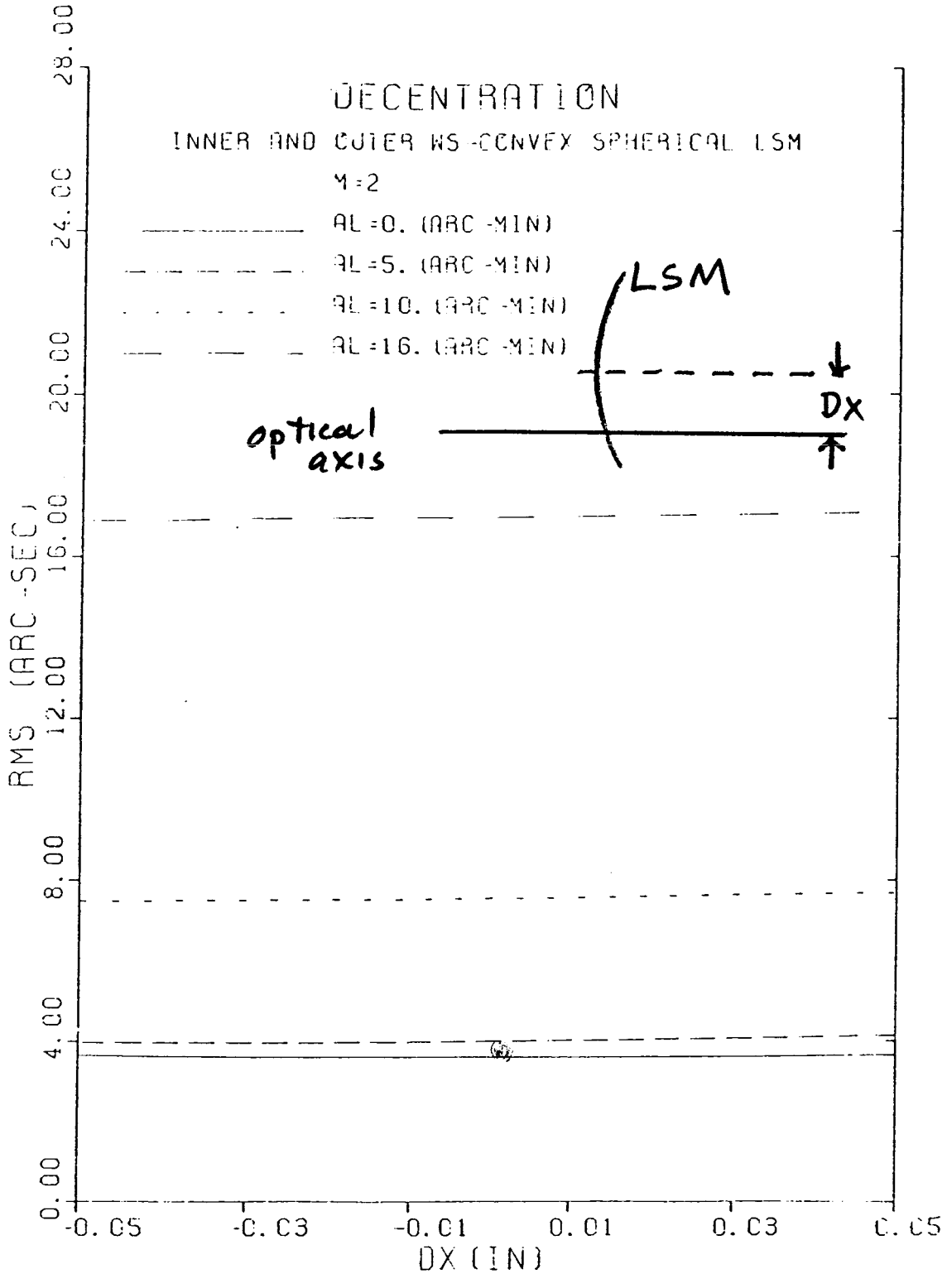

Figure 36. RMS blur circle radius versus the displacement of axis of LSM from the optical axis for Stanford/MSFC nested WS primary and convex spherical LSM secondary for M=2 and AL=0,5,10,16 arc-mins.

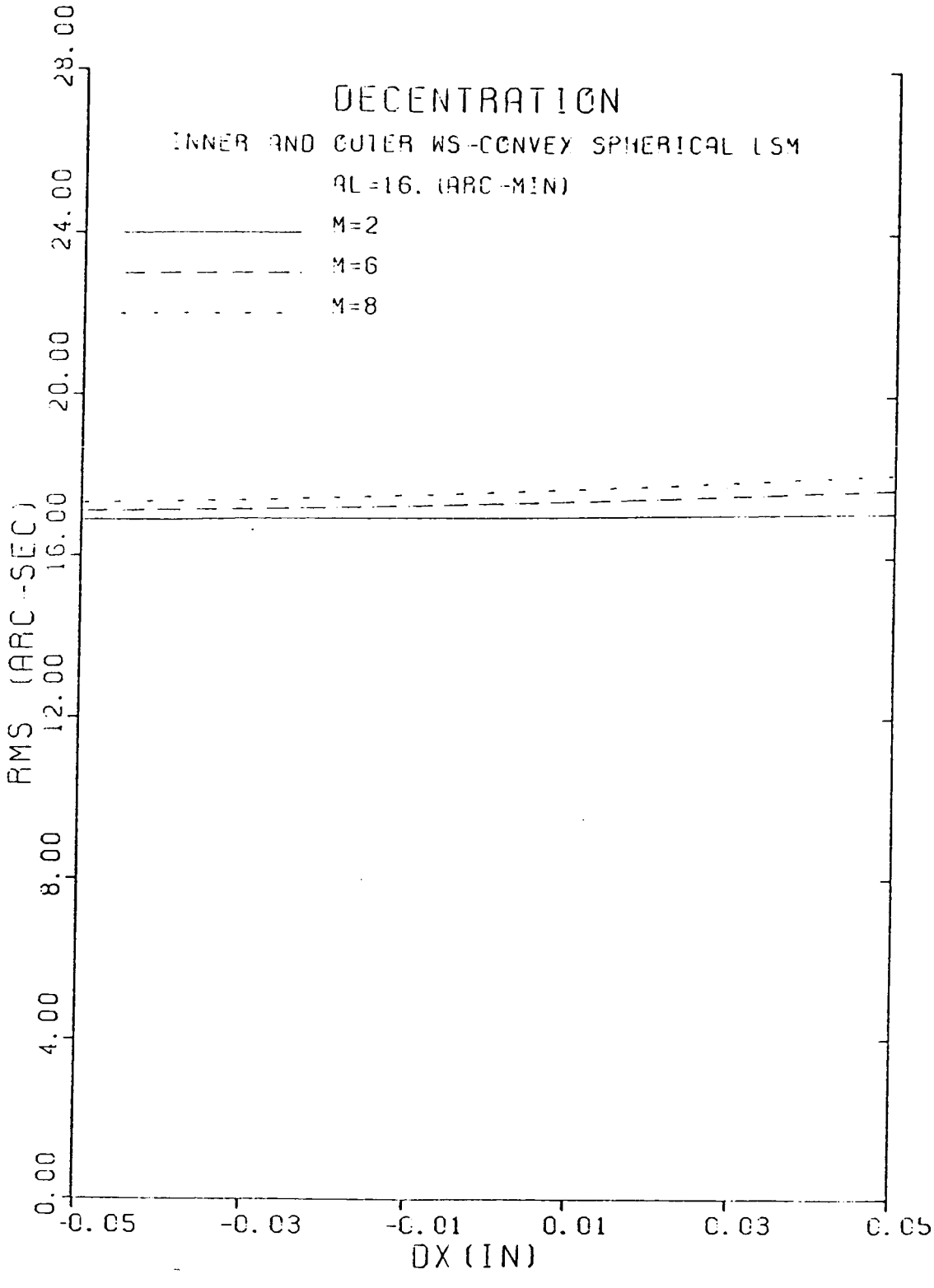

Figure 37. RMS blur circle radius versus the displacement of axis of LSM from the optical axis for Stanford/MSFC nested WS primary and convex spherical LSM secondary for M=2, 6,8 and AL=16 arc-mins.

Table 1. Primary Mirror Parameters

S-056 Wolter I		Wolter-Schwarzschild	
Focal Length	190.5 cm	Focal Length	128.2 cm
Glancing Angle	0.916	Glancing Angle	2.0 (outer mirror)
			1.7 (inner mirror)
Z max	392.76 cm		
Z min	380.62 cm	Inner Diameter	
Z min	369.19 cm	at Aperture	37.4 cm (outer mirror)
			33.0 cm (inner mirror)
r max	12.36 cm		
r min	12.17 cm	Element Lengths	26.7 (primary)
			21.8 cm (secondary)
A	95.02 cm		
B	4.31 cm	Collecting Area	107 cm (outer mirror)
C	95.25 cm		80 cm (inner mirror)
P	0.1946 cm		
Collecting Area	14.6 cm		

Table 2. Spectral Slicing X-Ray Telescope Systems (S-056)

LSM Optics	Field Angle (arc min)	FWHM (arc sec)* Meridional	Sagittal
SPHERICAL M = 2	on-axis	0.61	0.61
	1	0.59	0.59
	5	0.40	0.45
	10	0.16	0.21
	16	0.43	0.68
ELLIPSOIDAL M=2	on-axis	0.00	0.00
	1	0.004	0.004
	5	0.13	0.14
	10	0.58	0.59
	16	1.02	1.83
HYPERBOLOIDAL M = 2	on-axis	0.00	0.00
	1	0.004	0.005
	5	0.142	0.142
SPHERICAL M = 6	on-axis	0.24	0.24
	1	0.25	0.24
	5	0.035	0.055

*Full Width Half Maximum on Gaussian focal plane.